Finite elements based on Jacobi shape functions for the analysis of beams, plates and shells

Received: 2 December 2022 | Revised: 26 April 2023 | Accepted: 21 June 2023

DOI: 10.1002/nme.7316

RESEARCH ARTICLE

WILEY

Finite elements based on Jacobi shape functions for the analysis of beams, plates and shells

Alfonso Pagani | **Erasmo Carrera** | **Daniele Scano** | **Riccardo Augello**

Mul2 Lab, Department of Mechanical and Aerospace Engineering, Politecnico di Torino, Torino, Italy

Correspondence
Alfonso Pagani, Mul2 Lab, Department of Mechanical and Aerospace Engineering, Politecnico di Torino, Corso Duca degli Abruzzi 24, 10129 Torino, Italy.
Email: alfonso.pagani@polito.it

Funding information
Ministero dell'Università e della Ricerca

Abstract

This paper proposes the use of Jacobi polynomials to approximate higher-order theories of beam, plate, and shell structures. The Carrera unified formulation is used in this context to express displacement kinematics in a hierarchical form. In this manner, classical to complex higher-order theories can be implemented with ease. Particular attention is focused on the attenuation and the correction of the shear locking. Therefore, reduced integration as well as mixed interpolation of tensorial components methods are investigated against the new finite elements. Several case studies are taken into account to highlight the effectiveness and robustness of the proposed approach. Also, several benchmarks are provided for future assessments.

KEYWORDS

beam, Carrera unified formulation, finite element method, Jacobi polynomials, plate and shell models, shear locking

1 | INTRODUCTION

Modern advanced engineering, ranging from industrial applications to bio-mechanics, eventually requires complicated and computationally expensive structural analyses. For some geometries and to reduce the required computer power, appropriate one-dimensional (1D) and two-dimensional (2D) models can be adopted to analyze the three-dimensional (3D) continuum. The Finite Element Method (FEM) is undoubtedly the most important computational technique for structural analysis; see MacNeal,[1] who delineated the history of the FEM analysis.

In most Finite Element (FE) formulations, axiomatic-type theories are used. Concerning beam theories, Euler–Bernoulli Beam Model (EBBM)[2] and Timoshenko Beam Model (TBM)[3] represent classical formulations and are widely employed in the engineering practice. For both, the cross-section is considered to be rigid in its plane. Furthermore, the shear deformation is neglected in the case of EBBM, whereas it is considered constant along the cross-section in the case of TBM. Other beam FEs were developed in the last decades, see Reddy[4] and Carrera et al.[5] The most used 1D FEs shape functions to approximate either classical or high-order beam theories are those based on Lagrange polynomials. Eventually, two-, three- and four-node 1D FEs have been developed, see Bathe.[6] The same elements were used by Carrera et al.[7] to approximate models based on advanced kinematics and employing Carrera Unified Formulation (CUF).

If the 2D plate and shell elements are considered, Thin Plate Theory (TPT) and Thin Shell Theory (TST) represent the classical models. TPT and TST are based on Kirchhoff[8] hypotheses, which neglect transverse shear and trough-the-thickness deformation. In this manner, line segments perpendicular to the mid-plane so directed along the thickness direction remain orthogonal to the plate/shell reference surface during deformation. If the transverse shear

deformation is added in TPT or in TST for the shell case, the Reissner–Mindlin[9,10] theory can be provided. It is also commonly denoted as First-Order Shear Deformation Theory (FSDT). Although classical models do not satisfy the homogeneous condition at the top and bottom surfaces of plates/shells, they were the predominant structural theories in the early FEM plate/shell formulations, and some examples are given in Argyris.[11]

The majority of plate/shell FEs are based on Lagrange polynomials. Pryor and Barker[12] developed a four-node element for studying transverse shear effects. Parisch[13] provided a survey of the nine-node degenerated shell element. Furthermore, Bathe and Ho[14] reviewed several quadrilateral Lagrange-based elements: 4-, 8-, 9- and 16-node isoparametric shell elements. In particular, Carrera[15] used four-, eight- and nine-node FEs to study composite plates. Batoz et al.[16] studied a triangular three-node Lagrange-based element. Lee and Bathe[17] compared triangular plate/shell six- and seven-node elements with nine-node FEs.

Convergence alone is not enough to guarantee the numerical consistency of FE schemes although. FEs are affected by numerical problems when thin structures are analyzed, for example. Structures become excessively stiff in bending-dominant problems. This phenomenon is denoted as shear locking and leads to a severe increase in shear stiffness. The shear locking problem is a well-known issue, highlighted in many works. Several scientists presented methods to alleviate this behavior; see Reddy[4,18] and Crisfield.[19] Zienkiewicz, Taylor et al.[20] proposed the reduced integration scheme, for instance. In this method, the stiffness of elements is reduced by decreasing the order of the numerical integration in each term of the stiffness matrix. For example, Zlàmal[21] presented superconvergence and reduced integration in the plate/shell FEs. On the other hand, Prathat and Bhashyam[22] proposed a reduced integration for the beam elements. Another common technique is the so-called selective reduced integration scheme. This scheme is substantially a reduced integration for the transverse shear terms, whereas a full quadrature is employed for the remaining terms of the stiffness matrix, see Hughes et al.[23] These two integration schemes are powerful and increase the convergence rate displacement evaluation, but some spurious modes can appear, see MacNeal and Harder.[24] Dvorkin and Bathe[25] introduced a very diffused method based on mixed interpolation of shear strains. This method is commonly known as Mixed Interpolation of Tensorial Components (MITC). In particular, assumed strain distributions are here used for the derivation of the transverse shear terms. Bucalem and Bathe[26] remarked how this is a fully integrated method of the mixed interpolated element. The MITC technique has been extensively used for plate/shell formulation. Bathe and Dvorkin[27] proposed the so-called MITC4 and MITC8 with four- and eight-node Lagrange elements, respectively. Bucalem and Bathe[28] also presented 9- and 16-node Lagrange elements, that is, MITC9 and MITC16. Cinefra and Carrera[29] proposed a MITC9 shell element in the CUF framework. Bathe[6] presented a MITC method for alleviating shear locking in beam elements as well. In this work, a two-node Timoshenko beam FE is adopted. Lee et al.[30] proposed a geometry-dependent MITC method to avoid locking on two-node beam elements dealing with varying section beams. Carrera and Pagani[31] used a two-node Lagrange-like shape function in the CUF framework. Carrera et al.[32] extended the use also for three- and four- node beam elements.

Other FEs have been implemented to attenuate shear-locking issues. These FEs are based on anisoparametric (or interdependent) interpolation through Lagrangian polynomials. Tessler and Dong[33] implemented beam elements which include the effects of transverse shear deformation and rotary inertia. Concerning the plate elements, Tessler and Hughes[34] proposed a four-node, 12 degrees-of-freedom quadrilateral element based on Mindlin theory. Tessler and Hughes[35] implemented also a three-node triangular element based on the previous four-node element. Finally, Tessler[36] proposed reliable and simple shell elements. The bending part of the element is derived from Reissner–Mindlin plate, while Marguerre's shallow shell equations account for the membrane deformations and the membrane-bending coupling associated with the shell-element curvatures.

In the present paper, Jacobi polynomials are utilized as shape functions for beams, plates and shells. Jacobi polynomials are classical orthogonal polynomials, and they can be derived from a recurrence relation. They have the property to originate a vast class of polynomials changing the two parameters γ and θ; for example, Legendre and Chebyshev polynomials, see the book of Abramowitz and Stegun.[37] Interestingly FEs can be created using Jacobian shape functions, see Beuchler and Schöberl.[38] The use of this class of shape functions is not new, indeed. Fuentes et al.[39] proposed FEs based on shifted Jacobi polynomials, considering the parameter θ null. Several shapes were introduced for 1D, 2D, and 3D elements, as segments, quadrilaterals and tetrahedrons. Szabo, Duester et al.[40] suggested a hp-version of FE using hierarchical expansions derived from Legendre polynomials for beam, plate and solid. In this method, it is possible to increase both the number of elements, see Zhu and Zienkiewicz,[41] and the polynomial order of the shape function, see Babuška et al.[42]

Based on CUF, the present research introduces a new class of unified beam, plate and shell FEs based on Jacobi shape functions, with particular emphasis on the attenuation of numerical locking issues. Jacobi polynomials were used

to generate high order theories of structures in the framework of CUF in an axiomatic/asymptotic manner, see Carrera et al.[43] Low-order to very refined models were implemented. The latter were demonstrated to approximate the numerical and exact solutions in a very precise manner, eventually showing some interesting properties if compared to CUF-based Higher-Order Theories (HOT) employing Lagrange and Maclaurin thickness functions; see References 44-47. In the present work, instead, Jacobi polynomials are used to approximate the generalized displacements in the mid-plane in the case of plates and shells; that is, Jacobi polynomials are used here as shape functions in the framework of the FEM to provide approximate solutions given the theory approximation order. This paper is structured as follows: Section 2 briefly introduces Jacobi polynomials as shape functions. Formulation of the FEs for beams, plates, and shells is explained in Section 3. Section 4 presents the four benchmarks used in this paper for analysis. In Section 5, convergence and locking analyses are performed. Section 6 presents further results by adopting HOT. The capability of studying plate and shell structures of the beam formulation is illustrated in Section 7. Finally, Section 8 draws the most relevant conclusions of this work.

2 | SHAPE FUNCTIONS BASED ON JACOBI POLYNOMIALS

Lagrange-like shape functions are very popular in most of the FEM applications. In the present work, also several 1D and 2D Lagrange-like elements are used for assessing the new FEs. These elements are built by using a set of points which represent the roots of the polynomials themselves. As a matter of fact, Lagrange-based shape functions are not hierarchical. Thus, increasing the order of the model inevitably requires a remeshing. For instance, Figure 1 illustrates the position of nodes for four-node and sixteen-node 2D elements. For the purpose of completeness, Figure 2A shows two four-node beam elements, whereas Figure 3A depicts depicts a nine-noded elements mesh of a plate structure.

As the main objective of this paper, the Jacobi polynomials are adopted to build shape functions. One of the main attributes of these elements is their hierarchical nature. Enriched shape functions can be automatically built, indeed, by simply choosing the polynomial order p, while keeping the mesh fixed. Nevertheless, it is also possible to refine the mesh

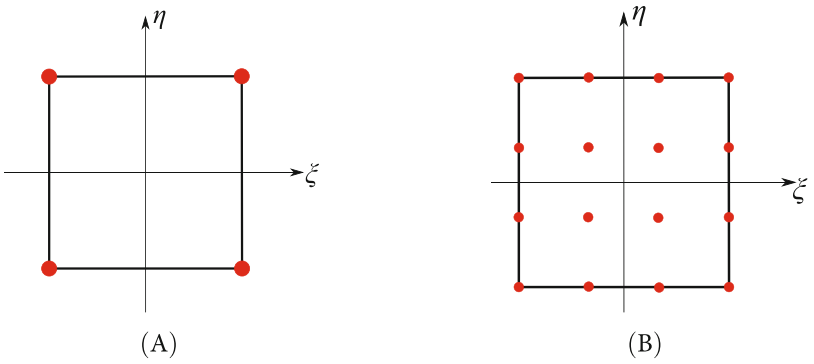

FIGURE 1 Four-node (A) and 16-node (B) two-dimensional Lagrange-like elements.

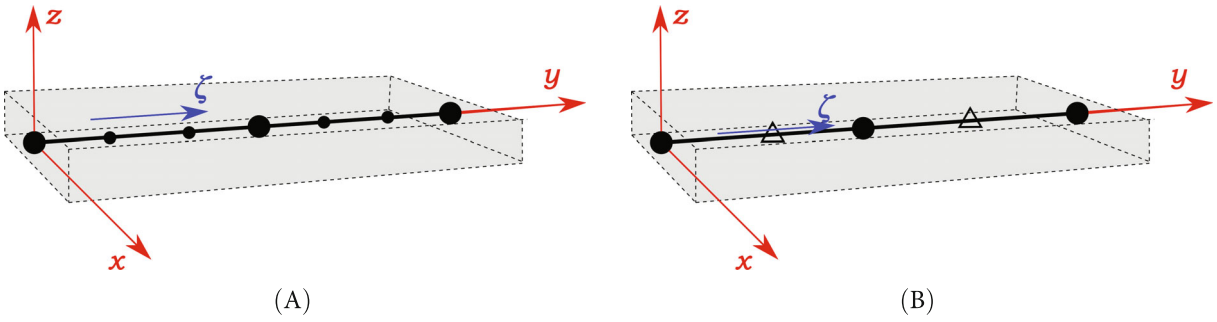

FIGURE 2 Beam elements for Lagrange (A) and Jacobi (B) shape functions.

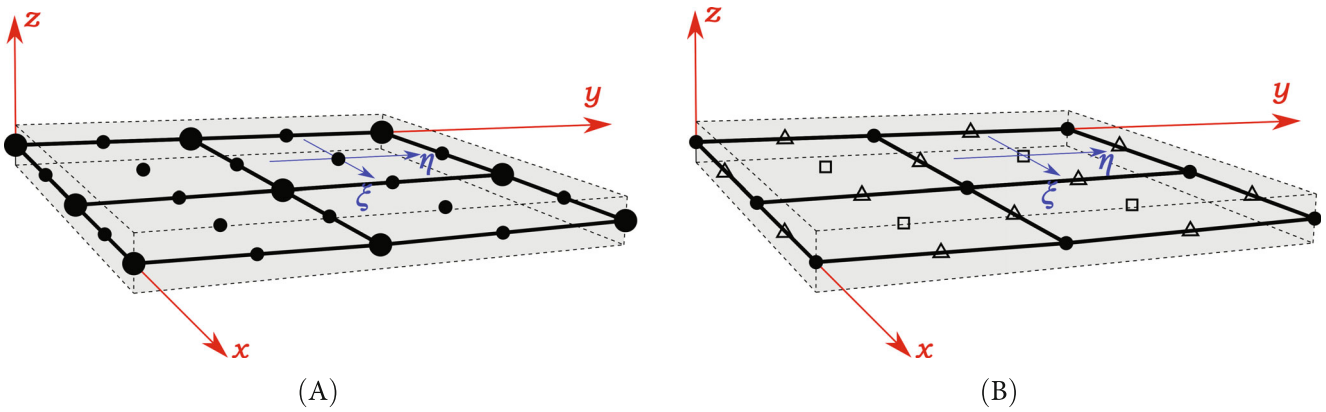

FIGURE 3 Plate/shell elements for Lagrange (A) and Jacobi (B) shape functions.

by increasing the number of FEs (h-refinement). Jacobi polynomials are formulated using recurrence relations, see the book of Abramowitz and Stegun.[37] The formula used to describe the orthogonal Jacobi polynomials is:

$$P_p^{(\gamma,\theta)}(\zeta) = \left(A_p\zeta + B_p\right) P_{p-1}^{(\gamma,\theta)}(\zeta) - C_p P_{p-2}^{(\gamma,\theta)}(\zeta), \tag{1}$$

where γ and θ are two scalar parameters and n is the order of the polynomial. The formula is calculated in natural plane $\zeta = [-1, +1]$. The first values are $P_0^{(\gamma,\theta)}(\zeta) = 1$ and $P_1^{(\gamma,\theta)}(\zeta) = A_0\zeta + B_0$. The parameters A_p, B_p, and C_p are:

$$\begin{aligned} A_p &= \frac{(2p+\gamma+\theta+1)(2p+\gamma+\theta+2)}{2(p+1)(p+\gamma+\theta+1)}, \\ B_p &= \frac{(\gamma^2-\theta^2)(2p+\gamma+\theta+1)}{2(p+1)(p+\gamma+\theta+1)(2p+\gamma+\theta)}, \\ C_p &= \frac{(p+\gamma)(p+\theta)(2p+\gamma+\theta+2)}{(p+1)(p+\gamma+\theta+1)(2p+\gamma+\theta)}. \end{aligned} \tag{2}$$

By choosing γ and θ, other popular polynomials can be devised. For example, Legendre polynomials are given by $\gamma = 0$ and $\theta = 0$.

2.1 | Application to beams

Figure 2B shows a FEM discretization with two elements along the beam axis. In this case, two kinds of polynomials are used along the y axis, one associated with nodes (or vertexes) and one associated with edges. In Figure 2B, ● represent the nodes for vertex expansions, whereas △ are the edge expansions. They are adopted as shape functions with the procedure described in Reference 40. There are two nodes and a number of edge modes which depend on the polynomial order of the element.

The hierarchic functions are defined as:

$$\begin{aligned} N_1(\zeta) &= \frac{1}{2}(1-\zeta) \\ N_2(\zeta) &= \frac{1}{2}(1+\zeta) \\ N_i(\zeta) &= \phi_{i-1}(\zeta), \quad i = 3, 4, \ldots, p+1, \end{aligned} \tag{3}$$

with

$$\phi_j(\zeta) = (1-\zeta)(1+\zeta) P_{j-2}^{\gamma,\theta}(\zeta), \quad j = 2, 3, \ldots, p, \tag{4}$$

where p indicates the polynomial order. The first two functions $N_1(\zeta)$, $N_2(\zeta)$ are the vertex expansions based on linear Lagrange polynomials. Given the following property

$$N_i(-1) = N_i(1) = 0, \quad i \geq 3, \tag{5}$$

the functions $N_i(\zeta), i = 3, 4, \ldots$ are denoted to as bubble functions or edge expansions.*

2.2 | Application to plates and shells

Figure 3B shows a FEM discretization with four elements for a plate structure. In this case three kinds of polynomials are used over the x-y plane: vertex (or node), edge and internal. There are four vertex modes and they vanish at all nodes but one. On the other hand, the number of edge modes depends on the polynomial order and they vanish for all sides of the domain but one. Finally, the internal modes are included from the fourth-order polynomial, and they vanish at all sides. ● represent the nodes for the vertex expansions, whereas △ are the edge expansions, and □ indicate the surfaces where internal expansions are defined. See Reference 48 for a similar procedure.

2.2.1 | Vertex expansions

The vertex modes correspond to the first-order, quadrilateral Lagrange polynomials:

$$N_i(\xi, \eta) = \frac{1}{4}(1 - \xi_i\xi)(1 - \eta_i\eta), \quad i = 1, 2, 3, 4, \tag{6}$$

where ξ and η are calculated in the natural plane between -1 and $+1$, and ξ_i and η_i are the vertex.

2.2.2 | Edge expansions

From $p \geq 2$, the edge modes arise in the natural plane as follows

$$\begin{aligned}
N_i(\xi, \eta) &= \frac{1}{2}(1 - \eta)\,\phi_p(\xi), \quad i = 5, 9, 13, 18, \ldots \\
N_i(\xi, \eta) &= \frac{1}{2}(1 + \xi)\,\phi_p(\eta), \quad i = 6, 10, 14, 19, \ldots \\
N_i(\xi, \eta) &= \frac{1}{2}(1 + \eta)\,\phi_p(\xi), \quad i = 7, 11, 15, 20, \ldots \\
N_i(\xi, \eta) &= \frac{1}{2}(1 - \xi)\,\phi_p(\eta), \quad i = 8, 12, 16, 21, \ldots
\end{aligned} \tag{7}$$

where p represents the polynomial degree of the bubble function $\phi_j(\zeta)$, already presented for the beam elements.

2.2.3 | Internal expansions

Introduced for $p \geq 4$, they vanish at all the edges of the quadrilateral domain. They sum $(p-2)(p-3)/2$ internal polynomials in total. By multiplying 1D edge modes, N_i internal expansions are built. For example, taking into account the set of fifth-order polynomials, it contains three internal expansions, which are

$$\begin{aligned}
N_{17}(\xi, \eta) &= \phi_2(\xi)\phi_2(\eta), \quad 2 + 2 = 4 \\
N_{22}(\xi, \eta) &= \phi_3(\xi)\phi_2(\eta), \quad 3 + 2 = 5 \\
N_{23}(\xi, \eta) &= \phi_2(\xi)\phi_3(\eta), \quad 2 + 3 = 5.
\end{aligned} \tag{8}$$

3 | FORMULATION OF FES

Consider the isotropic beam, plate and shell structures shown in Figure 4.

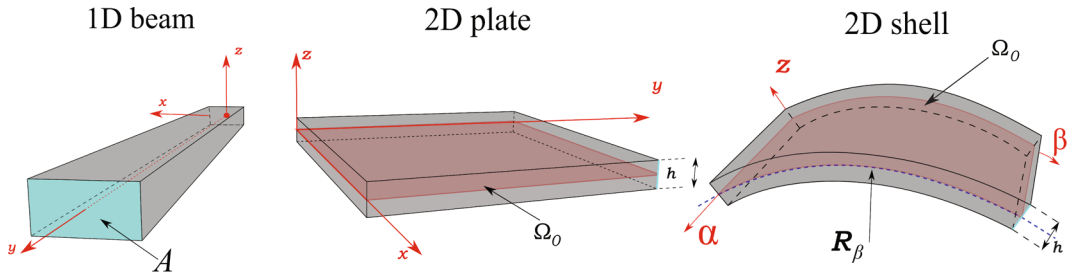

FIGURE 4 Generic beam, plate and shell structures. The one-dimensional beam and two-dimensional (2D) plate models (x, y, z) employs Cartesian reference system, whereas a curvilinear system (α, β, z) is used for the 2D shell model.

1D and 2D plate models adopt a Cartesian reference system. In particular, the cross-section A of the 1D model lays on the x-z plane. Thence, the beam axis is placed along the y direction. On the other hand, the 2D plate model uses the z coordinate for the thickness direction and the coordinates x and y indicate the in-plane mid-surface Ω_0. Finally, the shell uses a curvilinear reference frame (α, β, z) to account for the curvature, where α and β are the two in-plane directions. The 3D displacement fields are the followings:

$$\mathbf{u}(x,y,z) = \left\{ u_x \quad u_y \quad u_z \right\}^T, \quad \mathbf{u}(\alpha,\beta,z) = \left\{ u_\alpha \quad u_\beta \quad u_z \right\}^T. \tag{9}$$

Hereinafter, a brief review of the classical theories of beam, plate and shell is given. Note that no shear correction factors are used in this paper to overcome the well-known inconsistencies of the first-order shear models.

3.1 | Classical beam theories

The displacement field of the EBBM reads:

$$\begin{aligned} u_x(x,y,z) &= u_{x_1}(x,z) \\ u_y(x,y,z) &= u_{y_1}(x,y) - \frac{\partial u_{x_1}(y)}{\partial y} x + \frac{\partial u_{z_1}(y)}{\partial y} z \\ u_z(x,y,z) &= u_{z_1}(x,z). \end{aligned} \tag{10}$$

The displacement field of the TBM reads:

$$\begin{aligned} u_x(x,y,z) &= u_{x_1}(x,z) \\ u_y(x,y,z) &= u_{y_1}(x,z) + \phi_z(y)x - \phi_x(y)z \\ u_z(x,y,z) &= u_{z_1}(x,z), \end{aligned} \tag{11}$$

where u_{x_1}, u_{y_1}, and u_{z_1} represent the displacement of the beam axis, and ϕ_z and ϕ_x are the rotations around the z and x axes, respectively. Furthermore, $-\frac{\partial u_{x_1}(y)}{\partial y}$ and $\frac{\partial u_{z_1}(y)}{\partial y}$ are the rotations around the z and x axes when the cross-section remains plane and orthogonal to the line axis.

These theories work in a proper manner when slender, homogeneous beams with a compact section are taken into account.

3.2 | Classical plate theories

The displacement field of the TPT reads:

$$\begin{aligned} u_x(x,y,z) &= u_{x_1}(x,y) - \frac{\partial u_{z_1}(x,y)}{\partial x} z \\ u_y(x,y,z) &= u_{y_1}(x,y) - \frac{\partial u_{z_1}(x,y)}{\partial y} z \\ u_z(x,y,z) &= u_{z_1}(x,y). \end{aligned} \tag{12}$$

The displacement field of the FSDT reads:

$$\begin{aligned} u_x(x,y,z) &= u_{x_1}(x,y) + \phi_y(x,y)z \\ u_y(x,y,z) &= u_{y_1}(x,y) + \phi_x(x,y)z \\ u_z(x,y,z) &= u_{z_1}(x,y), \end{aligned} \tag{13}$$

where u_{x_1}, u_{y_1}, and u_{z_1} represent the displacement of the reference mid-surface of the plate, and ϕ_y and ϕ_x are the rotations around the y and x axes, respectively. On the other hand, $-\frac{\partial u_{z_1}(x,y)}{\partial x}$ and $-\frac{\partial u_{z_1}(x,y)}{\partial y}$ are the rotations around the y and x axes when the shear deformation is neglected.

When thin and homogeneous plates are studied, these theories work very well.

3.3 | Classical shell theories

The displacement field of the TPT reads:

$$\begin{aligned} u_\alpha(\alpha,\beta,z) &= u_{\alpha_1}(\alpha,\beta) - \frac{\partial u_{z_1}(\alpha,\beta)}{\partial \alpha} z \\ u_\beta(\alpha,\beta,z) &= u_{\beta_1}(\alpha,\beta) - \frac{\partial u_{z_1}(\alpha,\beta)}{\partial \beta} z \\ u_z(\alpha,\beta,z) &= u_{z_1}(\alpha,\beta). \end{aligned} \tag{14}$$

The displacement field of the FSDT reads:

$$\begin{aligned} u_\alpha(\alpha,\beta,z) &= u_{\alpha_1}(\alpha,\beta) + \phi_\beta(\alpha,\beta)z \\ u_\beta(\alpha,\beta,z) &= u_{\beta_1}(\alpha,\beta) + \phi_\alpha(\alpha,\beta)z \\ u_z(\alpha,\beta,z) &= u_{z_1}(\alpha,\beta), \end{aligned} \tag{15}$$

where u_{α_1}, u_{β_1} and u_{z_1} represent the displacement of the reference mid-surface of the shell, and ϕ_β and ϕ_α are the rotations around the β and α axes, respectively. Finally, $-\frac{\partial u_{z_1}(\alpha,\beta)}{\partial \alpha}$ and $-\frac{\partial u_{z_1}(\alpha,\beta)}{\partial \beta}$ are the rotations around the y and x axes when the shear deformation is neglected.

These theories work in a proper manner when thin and homogeneous shell are analyzed.

3.4 | Unified formulation for beam, plate, and shell and generalization to the HOT

The previous and more refined models can be described in a compact manner by using the CUF. The 3D displacement field is described as a generic expansion of the primary mechanical variables through the use of arbitrary functions of the domain:

$$\mathbf{u}(x,y,z) = F_\tau \mathbf{u}_\tau \quad \mathbf{u}(\alpha,\beta,z) = F_\tau \mathbf{u}_\tau \quad \tau = 1, 2, \ldots, M, \tag{16}$$

where F_τ are the expansion functions of the *generalized* displacements $\mathbf{u}_\tau$, where τ denotes summation and M is the order of expansion. The independent variables are explicitly shown for each formulation in Table 1. Thanks to this formalism, it is possible to choose a generic structural theory freely. In particular, HOTs were built from Taylor-like polynomials. When the beam formulation is considered, Taylor expansion uses 2D polynomials $x^i z^j$ as base, where i and j are positive integers. Carrera and Giunta[44] first studied beams from the first (T1) to the fourth (T4) order to account for nonclassical effects. On the other hand, for plates and shells, Taylor expansion adopts 1D polynomials z^i as base. Carrera[49] used several refined theories as a third-order theory (T3). Then, from the first-order Taylor expansion (T1), classical theories can be derived as degenerated cases. Carrera et al.[50] proposed a detailed explanation of the employed methods employed. For this reason, in the result section, the indicated DOFs are equal to those given for Taylor expansion of order 1, that is, nine for each node.

The CUF and the FEM can be used together to provide numerical results. In particular, FEM is adopted to discretize the generalized displacements $\mathbf{u}_\tau$. Thus, recalling equations described in Table 1, they are approximated as displayed in

TABLE 1 Carrera unified formulation (CUF) formulation.

Formulation	3D fields	CUF expansion	
1DBEAM :	$\mathbf{u}(x,y,z)$	$F_\tau(x,z)$	$\mathbf{u}_\tau(y)$
2DPLATE :	$\mathbf{u}(x,y,z)$	$F_\tau(z)$	$\mathbf{u}_\tau(x,y)$
2DSHELL :	$\mathbf{u}(\alpha,\beta,z)$	$F_\tau(z)$	$\mathbf{u}_\tau(\alpha,\beta)$

Note: τ denotes summation with $\tau = 1, 2, \ldots, M$, while M is the order of expansion.

TABLE 2 Finite element method.

Formulation	3D field	FEM+CUF expansions		
1DBEAM :	$\mathbf{u}(x,y,z)$	$N_i(y)$	$F_\tau(x,z)$	$\mathbf{q}_{\tau i}$
2DPLATE :	$\mathbf{u}(x,y,z)$	$N_i(x,y)$	$F_\tau(z)$	$\mathbf{q}_{\tau i}$
2DSHELL :	$\mathbf{u}(\alpha,\beta,z)$	$N_i(\alpha,\beta)$	$F_\tau(z)$	$\mathbf{q}_{\tau i}$

Note: i is repeated index with $i = 1, 2, \ldots, N$, where N is the number of shape functions per element.

Table 2, where N_i stand for the shape functions, the repeated subscript i indicates summation, N is the number of the shape functions per element and $\mathbf{q}_{\tau i}$ are the following vectors of the FE nodal parameters:

$$\mathbf{q}_{\tau i} = \left\{ q_{x_{\tau i}} q_{y_{\tau i}} q_{z_{\tau i}} \right\}^T \quad \mathbf{q}_{\tau i} = \left\{ q_{\alpha_{\tau i}} q_{\beta_{\tau i}} q_{z_{\tau i}} \right\}^T. \tag{17}$$

In this work, classical Lagrange-like and novel Jacobi FEs are used. When beam formulation is adopted, classical one-dimensional FEs with two-node (L2), three-node (L3) and four-node (L4) are used, that is, linear, parabolic, and cubic approximations along the y axis are assumed, respectively. Furthermore, the newly presented shape functions JP are adopted, where P is the polynomial order. In particular, J1, J2, J3, and J4 are used. For the 2D plate and shell formulations, classical two-dimensional FEs four-node (L4), nine-node (L9) and 16-node (L16), that is, linear, parabolic and cubic approximations over the x, y and α, β planes are assumed. Furthermore, the Jacobi shape functions J1, J2, J3, J4, and J5 are used.

The same shape functions are used for deflections, rotations, and higher-order terms. This aspect can be clearly seen in the equations.

Note that in this scenario, the geometric boundary conditions are applied directly to the 3D displacement components, independently of the theory approximation order. Those conditions are then projected to the available DOFs, with no loss of generality. The geometric boundary conditions are enforced with the same procedure for the three formulations. When the clamped condition is imposed, the translations along the three directions and the higher-order terms are fixed. On the contrary, the translations along the z and y (β) directions and the higher-order terms are fixed for the simply supported condition in plate and shell.

3.4.1 | Example for a beam element

Figure 5A shows the discretization for a beam model. J2 elements are adopted along the y axis and EBBM model is used as the structural theory. The displacement field for an element can be written as follows

$$\begin{aligned}
u_x(x,y,z) &= +\frac{1}{2}(1-y)\,q_{x_{11}} + \frac{1}{2}(1+y)\,q_{x_{12}} + (1-y)(1+y)\,q_{x_{13}} \\
&\quad + \frac{1}{2}(1-y)(1+y)\left[\gamma - \theta + (2+\gamma+\theta)\,y\right] q_{x_{14}}. \\
u_y(x,y,z) &= +\frac{1}{2}(1-y)\left(q_{y_{11}} - x q_{y_{21}} + z q_{y_{31}}\right) + \frac{1}{2}(1+y)\left(q_{y_{12}} - x q_{y_{22}} + z q_{y_{32}}\right) \\
&\quad + (1-y)(1+y)\left(q_{y_{13}} - x q_{y_{23}} + z q_{y_{33}}\right) \\
&\quad + \frac{1}{2}(1-y)(1+y)\left[\gamma - \theta + (2+\gamma+\theta)\,y\right]\left(q_{y_{14}} - x q_{y_{24}} + z q_{y_{34}}\right). \\
u_z(x,y,z) &= +\frac{1}{2}(1-y)\,q_{z_{11}} + \frac{1}{2}(1+y)\,q_{z_{12}} + (1-y)(1+y)\,q_{z_{13}} \\
&\quad + \frac{1}{2}(1-y)(1+y)\left[\gamma - \theta + (2+\gamma+\theta)\,y\right] q_{z_{14}}.
\end{aligned} \tag{18}$$

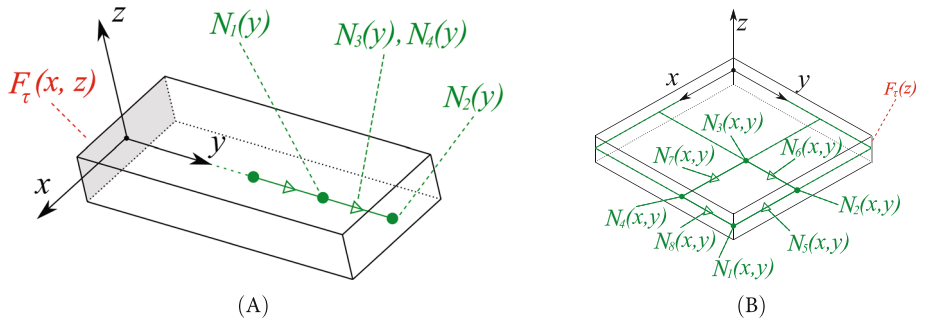

FIGURE 5 Finite element method discretization for beam (A) and plate (B) J2 elements.

For instance, when γ and θ are equal to zero, Legendre-like shape functions can be recovered.

3.4.2 | Example for a plate element

Figure 5B shows the discretization for a plate model. J2 elements are adopted in the x-y plane and TPT model is used as the structural theory. The displacement field for an element can be written as follows

$$\begin{aligned}
u_x(x,y,z) = &+\frac{1}{4}(1-x)(1-y)(q_{x_{11}} - zq_{x_{21}}) + \frac{1}{4}(1+x)(1-y)(q_{x_{12}} - zq_{x_{22}}) \\
&+ \frac{1}{4}(1+x)(1+y)(q_{x_{13}} - zq_{x_{23}}) + \frac{1}{4}(1-x)(1+y)(q_{x_{14}} - zq_{x_{24}}) \\
&+ \frac{1}{2}(1-y)(1-x^2)(q_{x_{15}} - zq_{x_{25}}) + \frac{1}{2}(1-y^2)(1+x)(q_{x_{16}} - zq_{x_{26}}) \\
&+ \frac{1}{2}(1+y)(1-x^2)(q_{x_{17}} - zq_{x_{27}}) + \frac{1}{2}(1-y^2)(1-x)(q_{x_{18}} - zq_{x_{28}}). \\
u_y(x,y,z) = &+\frac{1}{4}(1-x)(1-y)(q_{y_{11}} - zq_{y_{21}}) + \frac{1}{4}(1+x)(1-y)(q_{y_{12}} - zq_{y_{22}}) \\
&+ \frac{1}{4}(1+x)(1+y)(q_{y_{13}} - zq_{y_{23}}) + \frac{1}{4}(1-x)(1+y)(q_{y_{14}} - zq_{y_{24}}) \\
&+ \frac{1}{2}(1-y)(1-x^2)(q_{y_{15}} - zq_{y_{25}}) + \frac{1}{2}(1-y^2)(1+x)(q_{y_{16}} - zq_{y_{26}}) \\
&+ \frac{1}{2}(1+y)(1-x^2)(q_{y_{17}} - zq_{y_{27}}) + \frac{1}{2}(1-y^2)(1-x)(q_{y_{18}} - zq_{y_{28}}). \\
u_z(x,y,z) = &+\frac{1}{4}(1-x)(1-y)(q_{z_{11}}) + \frac{1}{4}(1+x)(1-y)(q_{z_{12}}) \\
&+ \frac{1}{4}(1+x)(1+y)(q_{z_{13}}) + \frac{1}{4}(1-x)(1+y)(q_{z_{14}}) \\
&+ \frac{1}{2}(1-y)(1-x^2)(q_{z_{15}}) + \frac{1}{2}(1-y^2)(1+x)(q_{z_{16}}) \\
&+ \frac{1}{2}(1+y)(1-x^2)(q_{z_{17}}) + \frac{1}{2}(1-y^2)(1-x)(q_{z_{18}}).
\end{aligned} \tag{19}$$

3.5 | Governing equations and FE matrices

According to the classical elasticity, stress, $\boldsymbol{\sigma}$, and strain, $\boldsymbol{\epsilon}$, tensors are expressed in vectorial form as follows:

$$\begin{aligned}
\boldsymbol{\sigma} &= \left\{ \sigma_{xx} \quad \sigma_{yy} \quad \sigma_{zz} \quad \sigma_{xz} \quad \sigma_{yz} \quad \sigma_{xy} \right\}^T, \quad \boldsymbol{\epsilon} = \left\{ \epsilon_{xx} \quad \epsilon_{yy} \quad \epsilon_{zz} \quad \epsilon_{xz} \quad \epsilon_{yz} \quad \epsilon_{xy} \right\}^T \\
\boldsymbol{\sigma} &= \left\{ \sigma_{\alpha\alpha} \quad \sigma_{\beta\beta} \quad \sigma_{zz} \quad \sigma_{\alpha z} \quad \sigma_{\beta z} \quad \sigma_{\alpha\beta} \right\}^T, \quad \boldsymbol{\epsilon} = \left\{ \epsilon_{\alpha\alpha} \quad \epsilon_{\beta\beta} \quad \epsilon_{zz} \quad \epsilon_{\alpha z} \quad \epsilon_{\beta z} \quad \epsilon_{\alpha\beta} \right\}^T.
\end{aligned} \tag{20}$$

The geometrical relations between strains and displacements can be defined as:

$$\boldsymbol{\epsilon} = \mathbf{b}\mathbf{u}, \tag{21}$$

where $\mathbf{b}$ is the matrix of differential operators, in the case of small displacements and angles of rotations, more information can be found in Carrera et al.[50,51]

Linear elastic isotropic materials are considered in this work and the constitutive relation becomes:

$$\boldsymbol{\sigma} = \mathbf{C}\boldsymbol{\epsilon}, \tag{22}$$

where $\mathbf{C}$ is the material elastic matrix, see Reference 6 and Hughes[52] for the explicit form.

The governing equations are derived from the Principle of Virtual Displacements and it reads:

$$\int_V (\delta\boldsymbol{\epsilon}^T\boldsymbol{\sigma})\mathrm{d}V = \delta L_e, \tag{23}$$

where V is the volume integration domain. The variation of the internal work is represented by the left-hand side of the equation, while the virtual variation of the external work is represented by the right-hand side.

Substituting the geometrical relations Equation (21), the constitutive Equation (22), and applying the CUF Table 1 and the FEM Table 2, the following governing equations are obtained:

$$\delta\mathbf{q}_{sj}^T : \mathbf{K}^{ij\tau s}\mathbf{q}_{\tau i} = \mathbf{P}_{sj}, \tag{24}$$

where $\mathbf{K}^{ij\tau s}$ is a 3×3 matrix, called fundamental nucleus of the mechanical stiffness matrix. $\mathbf{P}_{sj}$ is a 3×1 vector, called fundamental nucleus of the external load, see References 7 and 50.

In this paper, other than the full integration method, reduced, selective reduced and MITC are used in the governing equations. Both Lagrange-like and Jacobi-like shape functions are used for these numerical strategies. For reduced and selective reduced methods, the order of the numerical integration in certain terms of the stiffness matrix is decreased, see References 20 and 23. On the other hand, Appendix A presents an overview of the MITC methods for the 1D and 2D shape functions. This strategy uses assumed strain distributions for the derivation of the transverse shear terms. In this manner, the elements of the stiffness matrix are modified, see Reference 50.

4 | DESCRIPTION OF TEST CASES

The capabilities of the proposed FEs are assessed through four benchmarks, beam (B1), plate (B2), cylindrical shell (B3), and thin-walled cylinder (B4), and they are introduced in Sections 4.1–4.4. The numerical examples are compared to analytic and numerical solutions from the literature. In Section 5, a preliminary convergence analysis as a function of the Degrees of Freedom (DOF) is performed for metallic beam, plate, and shell cases, considering the shear locking effects. To overcome this issue, reduced, selective reduced and MITC integration techniques are addressed. Section 6 presents results by using HOT for studying even thicker beams, plates and shells accurately. In Section 7, the plate and the thin-walled cylinder are studied to demonstrate the advanced capabilities of the beam formulation. The proposed FEs are compared to classical linear, quadratic and cubic Lagrange-based ones. Several models can be created through the combination of FEM, integration schemes and structural theories.

In the figures and tables showing the results, several acronyms are used to recall specific FEs. In particular, concerning the shape functions, L*N* indicate Lagrange elements with *N* number of points, and J*P* are Jacobi shape functions where *P* is the polynomial order. When integration schemes are considered, *F* indicates full scheme, *S* indicates selective reduced scheme, *R* is for reduction scheme and *MITC*. As far as the structural theory is concerned, EBBM and TBM models are used. In the last result, higher-order Taylor expansions are employed as structural theories, and they are recalled as T*P*, where *P* indicates the order of the polynomial. Finally, the acronyms presented in the previous section are used if a classical model is adopted. Some examples are given:

- L4-*F*,T2: Four points Lagrange, full integration scheme, second-order Taylor.

TABLE 3 Geometrical and material properties of Benchmark 1.

Geometric description
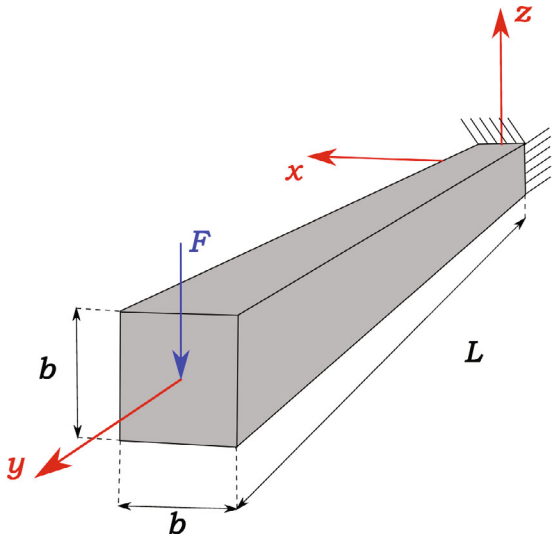
$L = 2$ m and $b = 0.2$ m
Material: $E = 75$ GPa, $\nu = 0.33$
Displacements: w [m]

Note: Metallic cantilever beam under transverse load.

TABLE 4 Metallic beam.

Beam theory	$w \times 10^5$ m
EBBM	5.333
TBM	5.369

Note: Results of classical beam theories.

- J2-*MITC*, EBBM: Second-order Jacobi, MITC integration scheme, Eulero-Bernoulli.

When comparing different formulations, the subscripts 1D, 2D and shell are written in the label for beams, plates, and shells, respectively.

4.1 | B1: Metallic beam

The first analysis case presented is a clamped beam subjected to a transverse force, as shown in Table 3, along with its geometric and material characteristics. The study case is taken from Reference 32. The cantilever beam is loaded toward the z-negative direction by a transverse force of module 200 N. The transverse displacement w is checked at the tip $[0, L, 0]$. Results are compared with those from Reference 32 and with classical solutions. Classical beam theories are adopted to obtain the analytical solution, see Table 4. No shear factor is used for both Analytical and FEM TBM solutions. This structure is analyzed with the 1D formulation.

4.2 | B2: Metallic plate

A metallic plate is analyzed as the second example. The geometric and loading conditions are described in Table 5. The plate is simply supported on the edges along the x-direction and it is loaded with a transverse sinusoidal pressure $p = p_z$

TABLE 5 Geometrical and material properties of Benchmark 2.

Geometric description
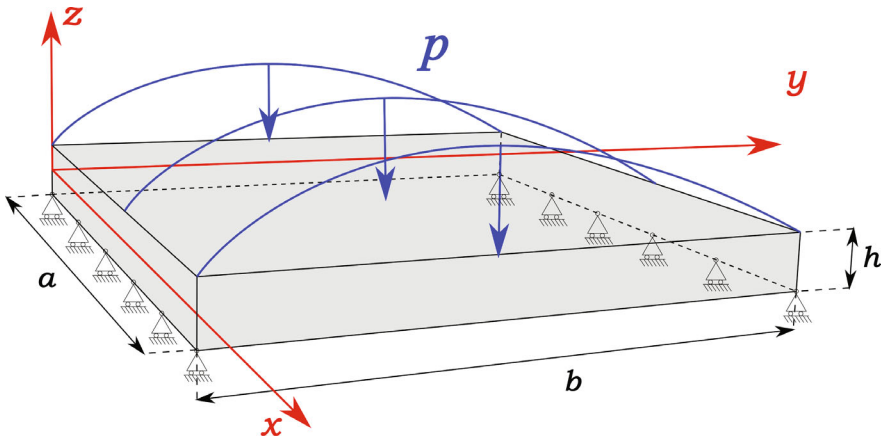
$b/h = 4,\ldots,1000$ and $a/b = 1$
Material: $E = 73$ GPa, $\nu = 0.34$
Non-dimensional displacements: $\overline{w} = \frac{100\ E\ w}{\left(\frac{b}{h}\right)^4 h\ p_z}$

Note: Simply supported metallic plate under distributed sinusoidal load.

$\sin\left(\frac{\pi y}{b}\right)$. The mechanical load amplitude at the top position is $p_z = 1$ Pa. Transverse nondimensional displacements $\overline{w}$ are evaluated in $[a/2, b/2, 0]$. Results are compared with a Navier-type, closed form solution, denoted as Exact. Given the strong-form governing equations, written in terms of the generalized displacements, that is, CUF DOF's in this paper, the Navier solution is analytical and employs two sinusoidal functions that satisfy the boundary condition in exact form. This is always possible in the case of simply supported structures with no mechanical couplings. A Taylor fourth-order theory is used along the thickness. See Reference 47 for more information. This structure is analyzed with the 2D formulation. Furthermore, a comparison between 1D and 2D formulations is made.

4.3 | B3: Metallic cylindrical shell

A cylindrical shell is considered as a further example. The geometric properties and loading conditions are reported in Table 6. The shell is simply supported on the longitudinal edges, and it is loaded with a transverse sinusoidal pressure $p = p_z \sin\left(\frac{\pi\beta}{b}\right)$ at the top. The mechanical load amplitude is $p_z = 1$ Pa. Transverse non-dimensional displacements $\overline{w}$ are calculated in $[a/2, b/2, 0]$. The reference solutions are given by a Navier-type, closed form solution derived from the strong form of the CUF for the shell formulation, as in the previous plate case. Along the thickness, a Taylor fourth-order theory is adopted. These solutions are labeled as Exact. See Reference 47 for more information. The shell is analyzed with the shell formulation.

4.4 | B4: Thin-walled cylinder

Finally, a thin-walled cylinder is considered, see Table 7 for the geometric and material characteristics. The structure is clamped on its edges. A transverse point load, F, is applied at $[0, L/2, R]$. F is equal to -5 MN. The analysis was originally proposed by Carrera et al.[53] The reference solution is given by Nastran shell model. In the reference paper, no information about the number of elements is given. However, because 6-DOF CQUAD elements are employed, there are reasonably

TABLE 6 Geometrical and material properties of Benchmark 3.

Geometric description
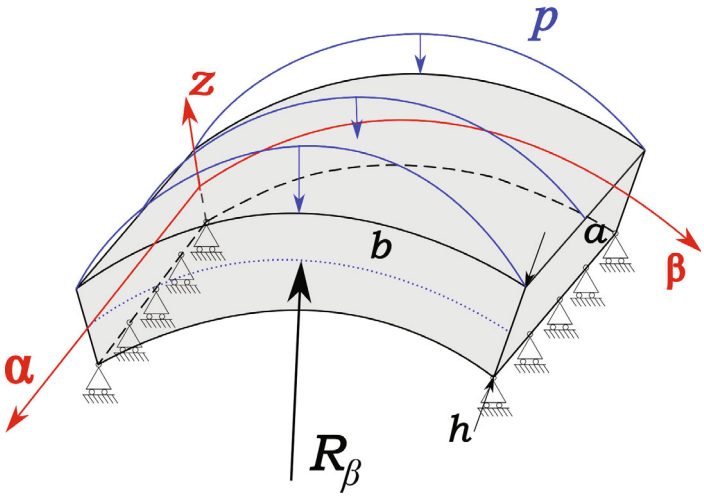
$R_\beta/b = \pi/3,\ R_\beta/h = 4, \ldots, 1000$ and $a/b = 1$
Material: $E = 73$ GPa, $\nu = 0.34$
Non-dimensional displacements: $\overline{w} = \dfrac{10\, E\, w}{\left(\frac{R_\beta}{h}\right)^4 h\, p_z}$

Note: Simply supported metallic shell under distributed sinusoidal load.

TABLE 7 Geometrical and material properties of Benchmark 4.

Geometric description
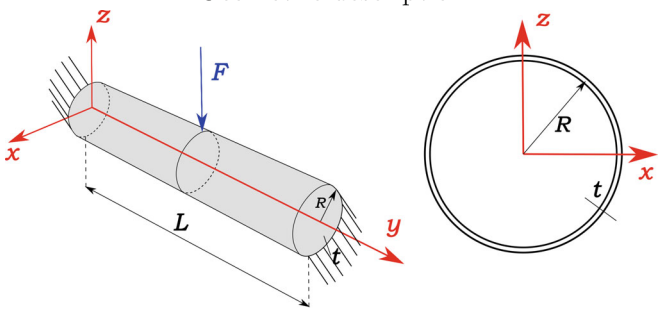
$R = 1$ m, $L = 2$ m and $t = 0.02$ m
Material: $E = 75$ GPa, $\nu = 0.33$
Displacements: w [m]

Note: Thin-walled shell under a point load.

around 2700 FEs. Transverse displacements w [m] are calculated at the mid-span $y = L/2$. Shell and 1D CUF results are compared with the reference solution.

5 | NUMERICAL ASSESSMENTS, CONVERGENCE, AND SHEAR LOCKING PROBLEMS

In this section, several convergence analyses for beams, plates, and shells have been performed to establish the numerical properties of the new presented shape functions.

5.1 | Metallic beam

As the first assessment for the beam FEs, a convergence of transverse displacements w is performed for a metallic cantilever beam, see Table 3. The results are compared with the classical exact solutions $w_{\text{Exact,EBBM}} = -5.333 \times 10^{-5}$ m and $w_{\text{Exact,TBM}} = -5.369 \times 10^{-5}$ m. Furthermore, transverse displacements are normalized as $\text{w}^* = w/w_{\text{Exact,EBBM}}$ or $\text{w}^* = w/w_{\text{Exact,TBM}}$. Three classical Lagrange shape functions, namely L2, L3, and L4 are compared with the proposed Jacobi shape functions, namely J1, J2, J3, and J4. Furthermore, four different integration schemes are used for every shape function. Finally, EBBM and TBM models are used as theories of structure. Figure 6 shows the convergence by using the EBBM kinematics and full integration schemes, while Figure 7 illustrates the convergence for the TBM model. Figures 8 and 9 show results for EBBM and TBM models, respectively. Only *MITC* integration scheme is illustrated since the same results can be obtained for selective reduced and reduced integration schemes.

Some remarks can be outlined from these results:

- FEs EBBM results converge to Exact, EBBM solution only if a great number of DOF is used due to the locking issues. Same consideration can be done for TBM theory.
- Shape functions with the same polynomial order show the same results, for example, second-order elements L3 and J2.
- L2-*F*,EBBM and J1-*F*,EBBM are very stiff elements. Both lead to a much slower rate of convergence. L2-*F*,TBM and J1-*F*,TBM show a faster convergence. Starting from the second-order elements, the convergence rate is very high for both EBBM and TBM.
- When adopting *S*, *R*, or MITC integration schemes, the results present the same trend convergence. This is valid for Lagrange as well as Jacobi shape functions. In addition, locking correction methods improve the behavior of L2 and J1 elements.

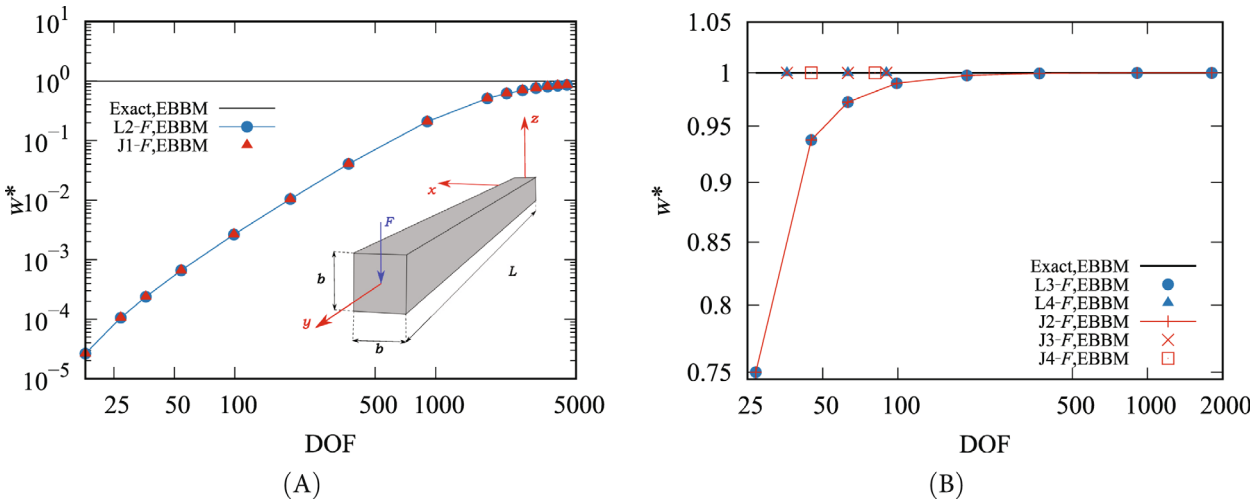

FIGURE 6 Metallic beam. Convergence of transverse displacements $\text{w}^* = w/w_{\text{Exact,EBBM}}$ in $[0, L, 0]$ with one-dimensional formulation using Euler–Bernoulli beam model (EBBM) and full integration scheme.

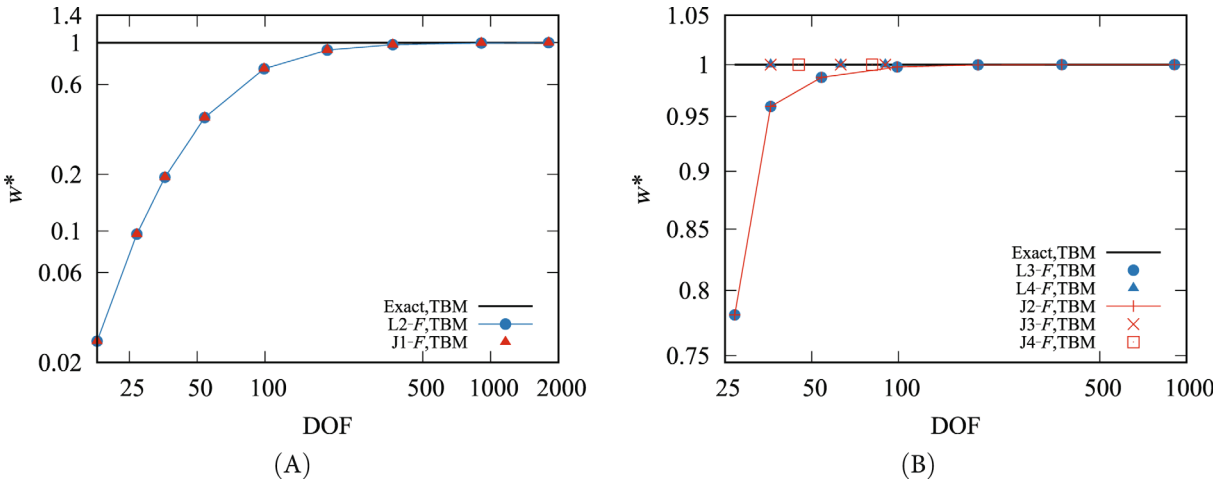

FIGURE 7 Metallic beam. Convergence of transverse displacements $w^* = w/w_{\text{Exact,TBM}}$ in $[0, L, 0]$ with 1D formulation by using Timoshenko beam model (TBM) and full integration scheme.

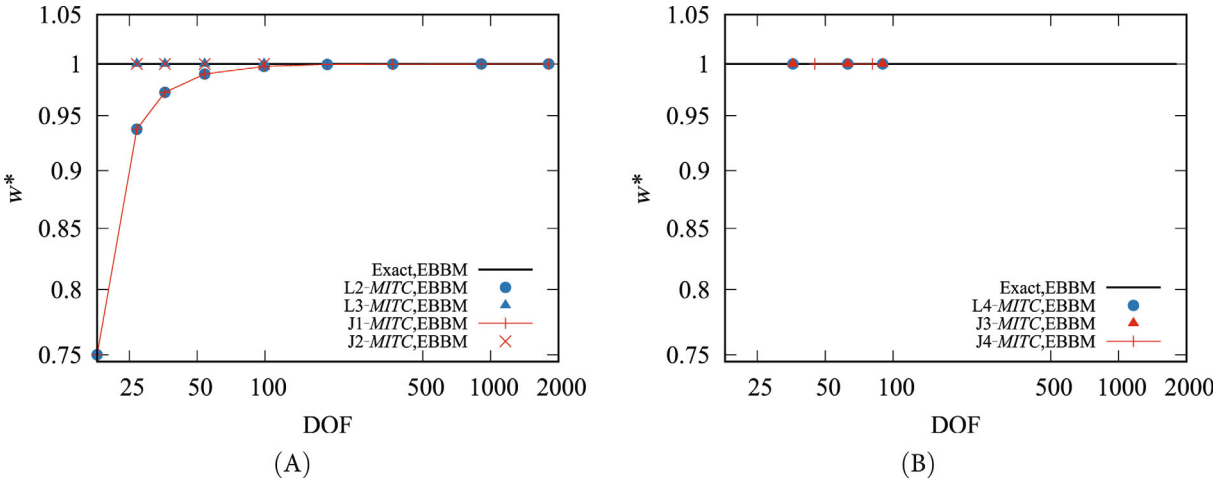

FIGURE 8 Metallic beam. Convergence of transverse displacements $w^* = w/w_{\text{Exact,EBBM}}$ in $[0, L, 0]$ with one-dimensional formulation using Euler–Bernoulli beam model (EBBM) and mixed interpolation of tensorial components integration scheme.

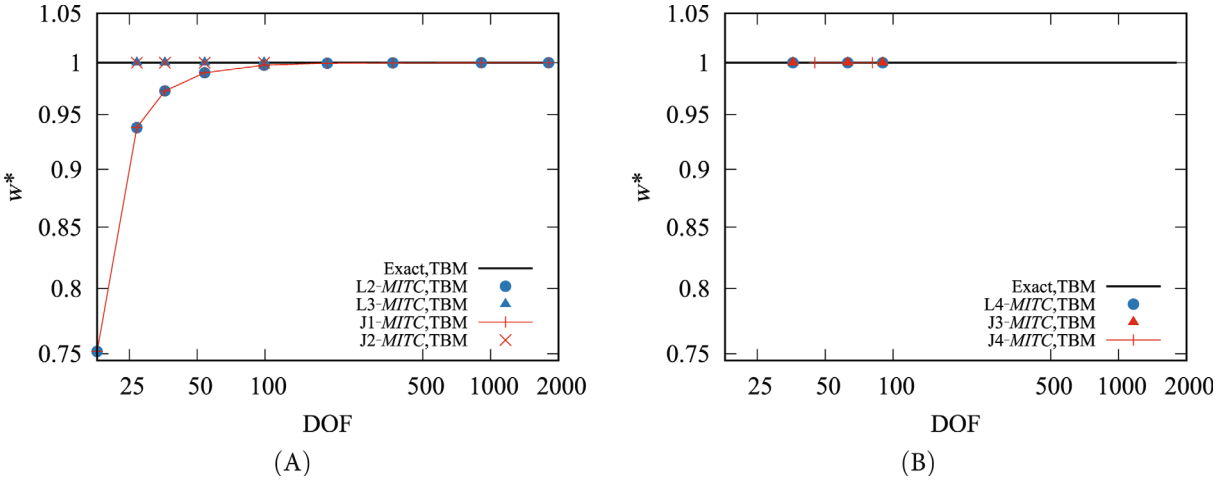

FIGURE 9 Metallic beam. Convergence of transverse displacements $w^* = w/w_{\text{Exact,TBM}}$ in $[0, L, 0]$ with one-dimensional formulation by using Timoshenko beam model (TBM) and mixed interpolation of tensorial components integration scheme.

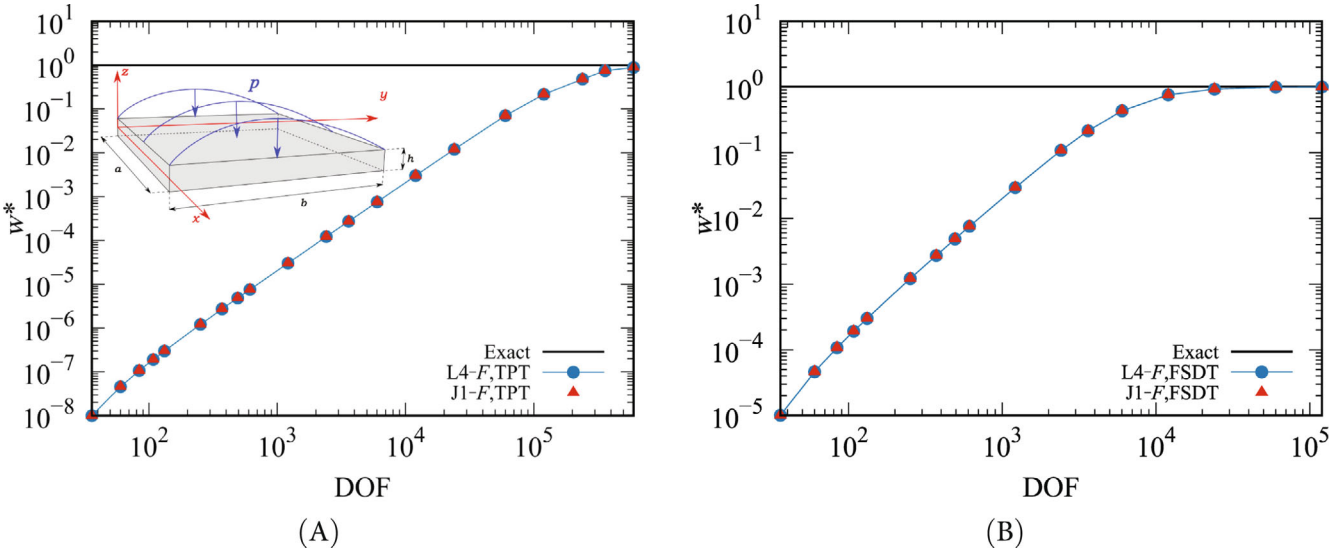

FIGURE 10 Metallic plate, case $b/h = 1000$. Convergence of transverse displacements $w^* = \overline{w}/\overline{w}_{\text{Exact}}$ in $[a/2, b/2, 0]$ with two-dimensional formulation by using full integration scheme for L4 and J1.

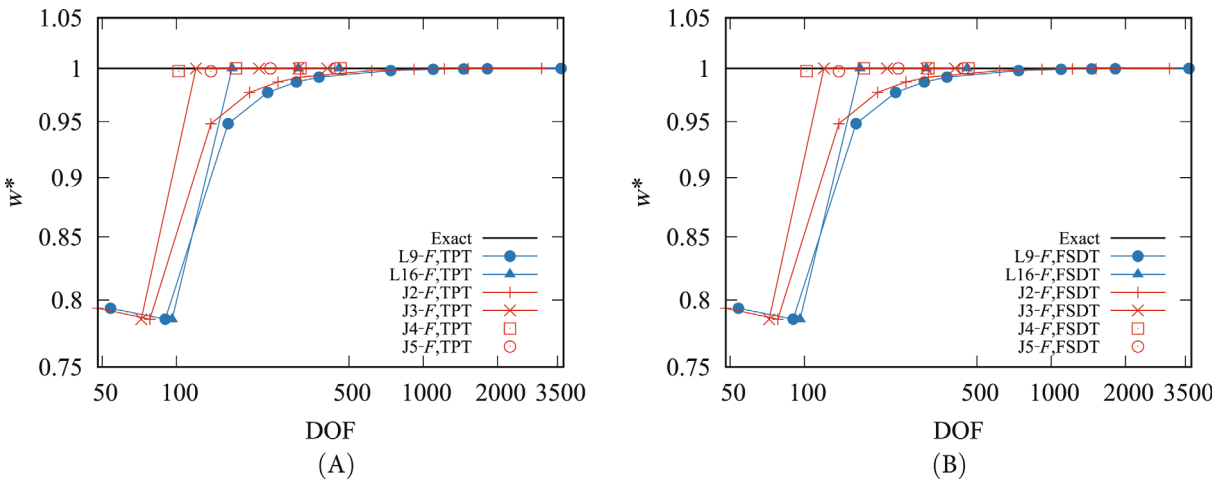

FIGURE 11 Metallic plate, case $b/h = 1000$. Convergence of transverse displacements $w^* = \overline{w}/\overline{w}_{\text{Exact}}$ in $[a/2, b/2, 0]$ with two-dimensional formulation by using full integration scheme.

5.2 | Metallic plate

The performances of the plate FEs are studied through the convergence analysis of transverse displacements for a thin simply-supported metallic plate, with a length-to-thickness ratio $b/h = 1000$, see Table 5. The results are compared with a closed form solution $\overline{w}_{\text{Exact}} = 10.895$. Furthermore, transverse displacements are normalized through the following expression: $w^* = \overline{w}/\overline{w}_{\text{Exact}}$. Three classical Lagrange shape functions, namely L4, L9 and L16 are compared with the proposed Jacobi shape functions, namely J1, J2, J3, J4, and J5. Full, reduced, and selective reduced integration schemes are used for all the shape functions, while MITC is not implemented for J4 and J5. Finally, classical structural theories TPT and FSDT are used. Figure 10 shows the convergence using the TPT kinematics and full integration scheme, while Figure 11 illustrates the convergence for the FSDT model. Figure 12 shows the results for TPT and selective reduced integration scheme. Only selective reduced integration scheme is illustrated since the same results can be obtained for reduced integration schemes. Figure 13 shows the results for TPT and MITC integration scheme. Since TPT and FSDT yield the same results, only the first theory is shown.

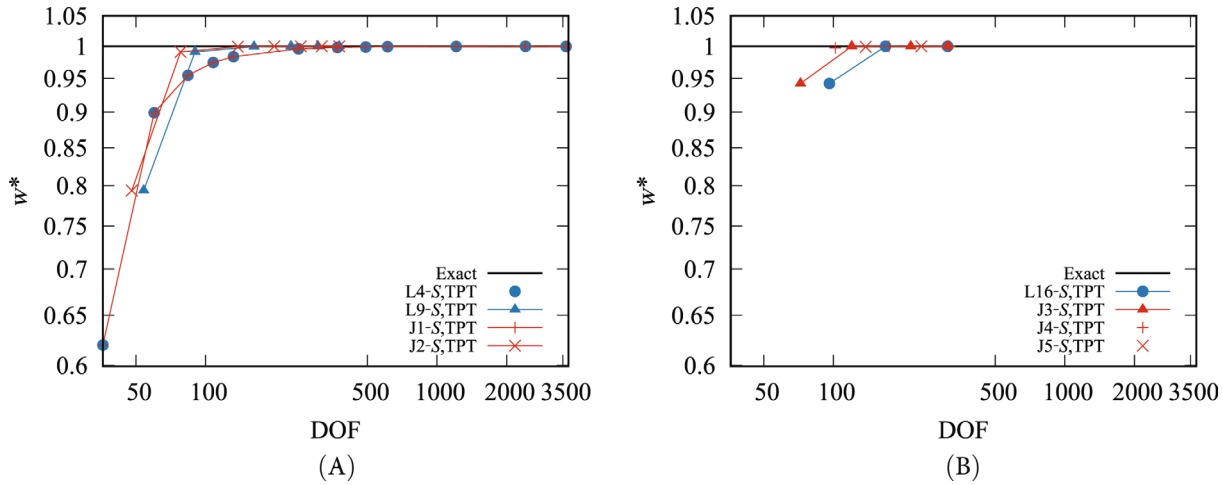

FIGURE 12 Metallic plate, case $b/h = 1000$. Convergence of transverse displacements $w^* = \overline{w}/\overline{w}_{\text{Exact}}$ in $[a/2, b/2, 0]$ with two-dimensional formulation by using thin plate theory and selective integration scheme.

The following considerations can be made at the end of the analysis:

- Shape functions with the same polynomial order present a similar convergence trend, for example, second-order elements L9 and J2. In particular, Jacobi FEs show the same results with less DOF. However, L4 and J1 present the same results.
- L4-*F*,TPT and J1-*F*,TPT are very stiff elements. Both reach the convergence when many DOFs are used. On the other hand, L4-*F*,FSDT and J1-*F*,FSDT are slightly faster. Starting from the third-order elements, the convergence rate is very high. J4 and J5 shape functions are near to the exact solution with only one element.
- When adopting selective reduced, reduced or MITC integration schemes, the results present the same trend convergence. This is valid for Lagrange as well as Jacobi shape functions. Locking correction methods improve the behavior of L4, L9, L16, J1, J2 and J3 elements. In these cases, TPT and FSDT present the same results.

5.3 | Metallic shell

As the first assessment for the shell elements, a convergence analysis of transverse displacements w is performed for a thin simply supported metallic shell, see Table 6. The radius-to-thickness ratio R_β/h is set to 1000. The results are compared with a closed form solution $\overline{w}_{\text{Exact}} = 1.6591$. The expression $w^* = \overline{w}/\overline{w}_{\text{Exact}}$ is used to normalize the transverse displacements. Three classical Lagrange shape functions, namely L4, L9, and L16 were compared with the newly presented Jacobi shape functions, namely J1, J2, J3, J4, and J5. Full, reduced, and selective reduced integration schemes are adopted for all the shape functions, while *MITC* is not implemented for J4 and J5. Concerning the structural theories, classical structural theories TST and FSDT are used. Figure 14 shows the convergence by using the TST kinematics and full integration scheme, while Figure 15 illustrates the convergence for the FSDT model. Figure 16 shows the results for reduced integration scheme. Finally, Figures 17 and 18 illustrate the convergence for selective reduced and MITC integration schemes. TST results are shown because both classical theories yield the same results.

The following considerations can be drawn:

- As seen in the plate analysis, shape functions with the same polynomial order present a similar convergence trend. In particular, Jacobi FEs have a faster convergence rate. In fact, they yield better results with less DOFs. On the other hand, L4 and J1 show the same behavior.
- L4-*F*,TST and J1-*F*,TST reach the convergence for elevated number of DOFs because these shape functions are bilinear elements. On the other hand, L4-*F*,FSDT and J1-*F*,FSDT are slightly faster. When L9 and J2 elements are used, a better convergence rate is shown. The convergence rate is very high if third-, fourth- and fifth-order elements are adopted. In, particular, J4 and J5 shape functions are near to the exact solution with only one element.

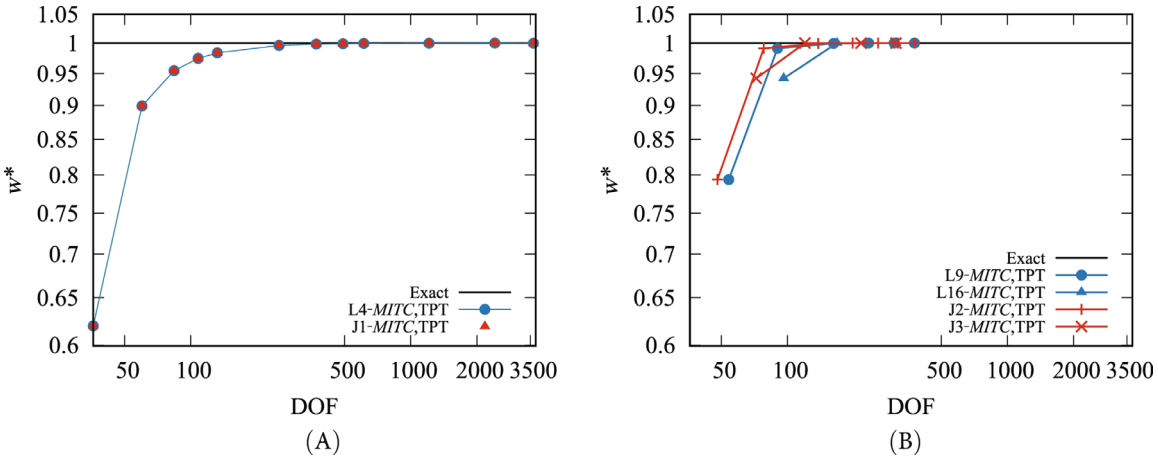

FIGURE 13 Metallic plate, case $b/h = 1000$. Convergence of transverse displacements $w^* = \overline{w}/\overline{w}_{\text{Exact}}$ in $[a/2, b/2, 0]$ with 2D formulation by using thin plate theory and mixed interpolation of tensorial components integration scheme.

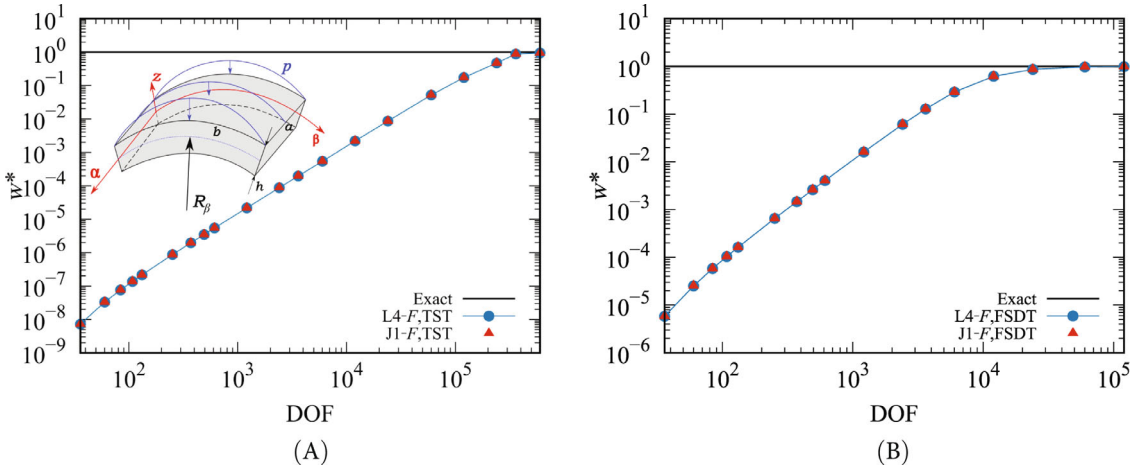

FIGURE 14 Metallic shell, case $R_\beta/h = 1000$. Convergence of transverse displacements $w^* = \overline{w}/\overline{w}_{\text{Exact}}$ in $[a/2, b/2, 0]$ with shell formulation by using full integration scheme for L4 and J1.

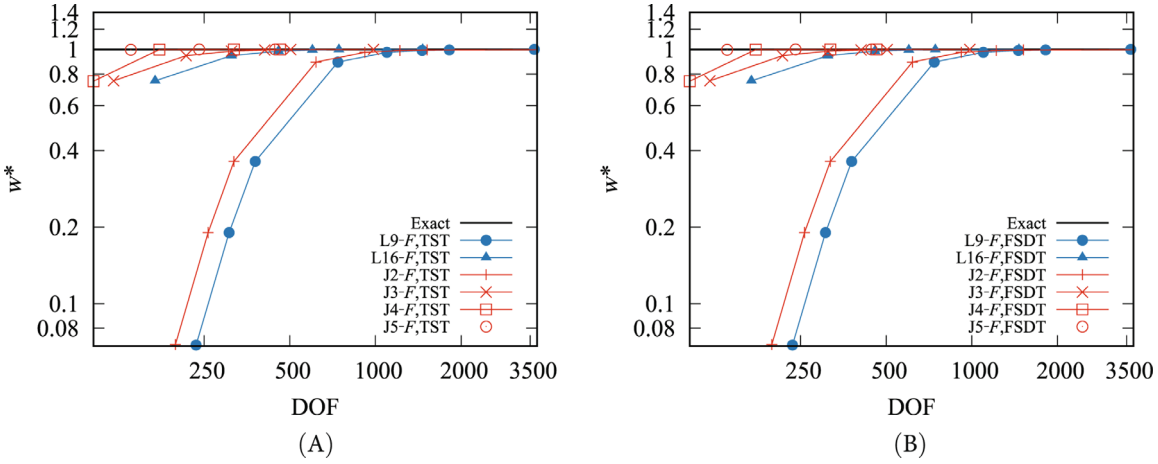

FIGURE 15 Metallic shell, case $R_\beta/h = 1000$. Convergence of transverse displacements $w^* = \overline{w}/\overline{w}_{\text{Exact}}$ in $[a/2, b/2, 0]$ with shell formulation by using full integration scheme.

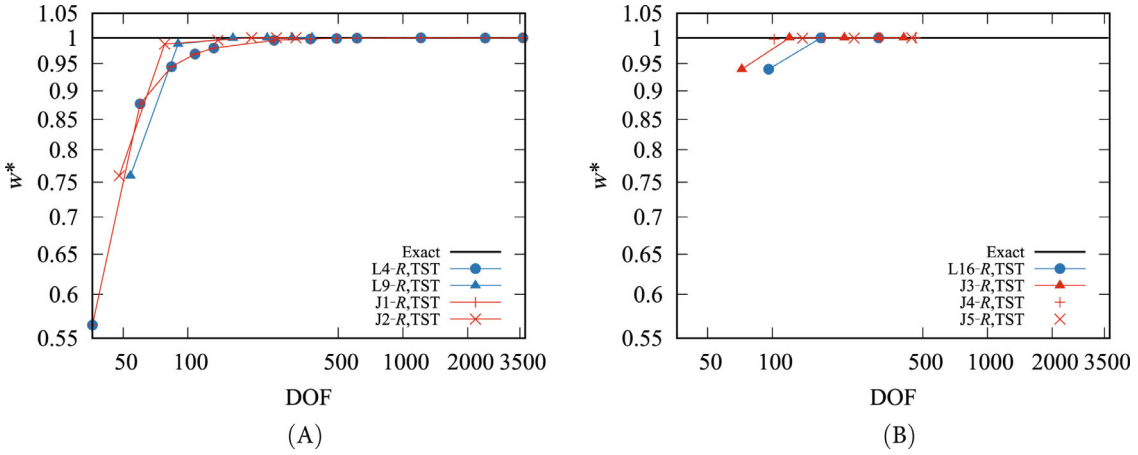

FIGURE 16 Metallic shell, case $R_\beta/h = 1000$. Convergence of transverse displacements $w^* = \overline{w}/\overline{w}_{\text{Exact}}$ in $[a/2, b/2, 0]$ with shell formulation by using reduced integration scheme.

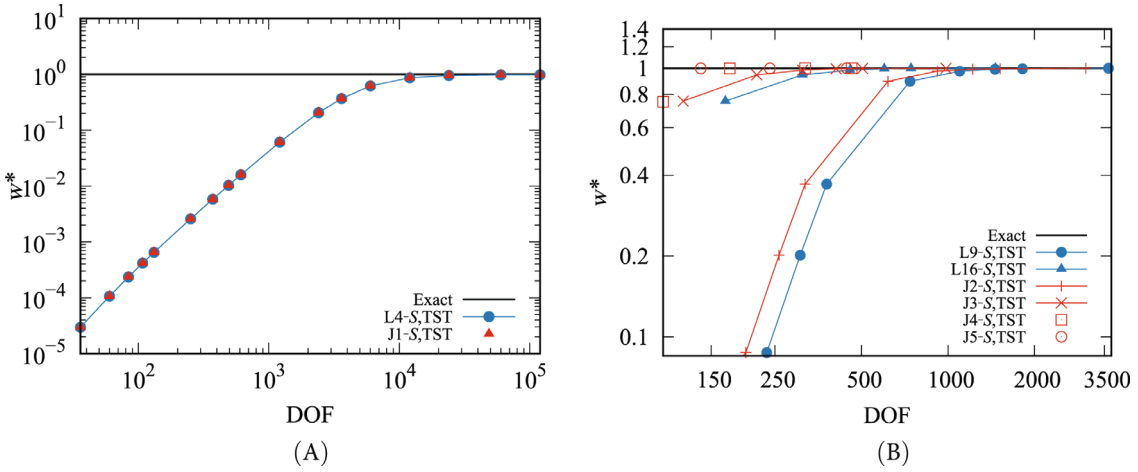

FIGURE 17 Metallic shell, case $R_\beta/h = 1000$. Convergence of transverse displacements $w^* = \overline{w}/\overline{w}_{\text{Exact}}$ in $[a/2, b/2, 0]$ with shell formulation by using selective integration scheme.

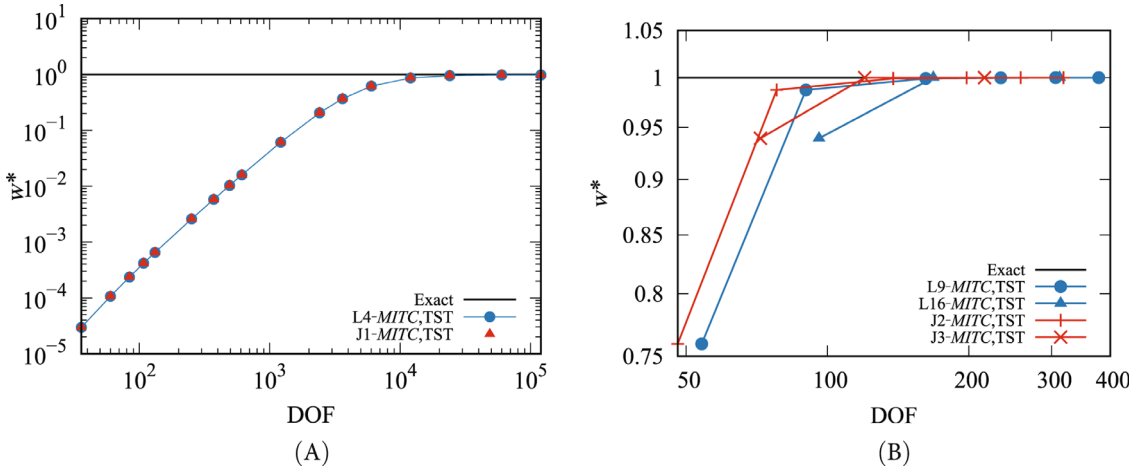

FIGURE 18 Metallic shell, case $R_\beta/h = 1000$. Convergence of transverse displacements $w^* = \overline{w}/\overline{w}_{\text{Exact}}$ in $[a/2, b/2, 0]$ with shell formulation by using mixed interpolation of tensorial components integration scheme.

- Reduced integration schemes show improvements for all the theories adopted. When adopting the same shape functions, results for selective reduced, reduced, or MITC integration schemes present the same trend convergence. Locking correction methods improve the behavior of L4, L9, L16, J1, J2, and J3 elements. In these cases, TPT and FSDT present the same results.

6 | THE CASES OF HIGHER-ORDER BEAM, PLATE, AND SHELL

In this section, the new Jacobi-like shape functions have been used with higher-order structural theories.

6.1 | Metallic beam

After studying the behavior of classical theories, HOT are employed to analyze the beams. Again, a metallic cantilever beam is taken into account, see Table 3 for the properties. Transverse displacements at the tip section are evaluated. The results are compared with two solutions from Carrera et al.[32] In the reference, L9 expansion was used as the cross-section model. See[50] for more information on the use of Lagrange-based structural theories. The reference solutions from Reference 32 are compared with the classical Lagrangian shape functions and the Jacobi FEs. Full and MITC integration schemes are adopted. In the present paper, a second-order Taylor (T2) expansion is used as the structural theory. Each node has 6×3 DOFs, where 6 is the number of terms of the Taylor polynomial of order 2, and 3 stands for u_x, u_y, and u_z. The DOFs of the first node (at clamped end) vanish for all the directions. Table 8 shows the results for several FEM models. Furthermore, DOFs and Number of FEs (N^{o}_{FEM}) are given for comparison purposes. DOF used for each model are near to those adopted for J4.

The analysis of the beam highlights the following statements:

- For the HOTs, it is confirmed that the shape functions with the same polynomial order present similar results, for example, second-order elements L3 and J2.
- MITC integration scheme is confirmed to be a powerful method to contrast the shear locking phenomenon also for Jacobi elements.
- J4-*F* and J4-*MITC* present the same results, demonstrating that very refined FEs can resolve locking problems. Furthermore, their results are near the MITC reference solution, even though lesser DOFs are used.

TABLE 8 Metallic beam.

Element type	$-w \times 10^5$ m	DOF	N^{o}_{FEM}
L2-*F*[32]	5.311	5427	200
L2-*MITC*[32]	5.316	5427	200
T2			
L2-*F*	5.177	738	40
L2-*MITC*	5.185	738	40
J1-*F*	5.177	738	40
J1-*MITC*	5.185	738	40
L3-*F*	5.305	738	20
L3-*MITC*	5.306	738	20
J2-*F*	5.305	738	20
J2-*MITC*	5.306	738	20
J4-*F*	5.312	738	10
J4-*MITC*	5.312	738	10

Notes: Transverse displacements in $[0, L, 0]$ with one-dimensional formulation using T2 kinematic model. N^{o}_{FEM} is the number of finite elements.

6.2 | Metallic plate

Also, HOT can be adopted for the plate elements to study structures in some cases. Again, a metallic simply supported plate is taken into account, see Table 5 for the properties. Transverse displacements at the center of the plate are evaluated. A number of length-to-thickness ratios are considered, namely $b/h = 4, 10, 100, 1000$. The reference solutions are given by closed-form 2D models (Exact). The reference solutions are compared with the classical Lagrangian shape functions and the Jacobi FEs. Full integration scheme is adopted. As far as the structural theory is concerned, a fifth-order Taylor (T5) expansion is used to accurately study plates with different thicknesses. Each node has 6×3 DOFs, where 6 is the number of terms of the Taylor polynomial of order 5, and 3 stands for u_x, u_y, and u_z. The DOFs of the nodes along the simply supported edges vanish along the directions. Table 9 shows the results for several FEM models. Furthermore, DOFs and Number of FEs (N^{o}_{FEM}) are given for comparison purposes. DOF used for each model are near to those adopted for J5.

The analysis of the plate leads to the following conclusions:

- It is confirmed that the shape functions with the same polynomial order and equal DOF are invariant with respect to the solution accuracy.
- L4 and J1 are progressively far from the reference solution when the length-to-thickness ratio increases. Locking problems also affect L9 and J2, but with less intensity. Furthermore, J2 shows slightly better behavior than L9.
- L16, J3, J4 and J5 can approach the reference solution for each length-to-thickness ratio, showing that they are locking-free.

6.3 | Metallic shell

HOT are adopted to study shells with different radius-to-thickness ratios, namely $R_\beta/h = 4, 10, 50, 100, 1000$. Again, a metallic simply-supported shell is considered, see Table 6 for the properties. Transverse displacements at the center of the shell are evaluated. The reference solutions are given by closed-form two-dimensional models (Exact). The reference solutions are compared with the classical Lagrangian shape functions and the Jacobi FEM elements. Full integration scheme is adopted. A fifth-order Taylor (T5) expansion is used as the structural theory to capture the behavior in the case of thick structure. The number of DOFs and the boundary conditions are the same as in the plate case. Table 10 shows the results for several FEM models. DOFs and Number of FEs (N^{o}_{FEM}) are indicated to make comparisons. DOF used for each model are near to those adopted for J5.

TABLE 9 Metallic plate.

b/h	4	10	100	1000	DOF	N^{o}_{FEM}
Element type						
Exact —	**12.656**	**11.179**	**10.897**	**10.895**	—	—
T5						
L4	12.564	10.891	3.0708	0.0426	1332	36
J1	12.564	10.891	3.0708	0.0426	1332	36
L9	12.655	11.176	10.836	10.811	1350	12
J2	12.656	11.178	10.856	10.834	1314	14
L16	12.656	11.179	10.898	10.895	1368	6
J3	12.656	11.179	10.898	10.895	1368	9
J4	12.656	11.179	10.898	10.895	1386	6
J5	12.657	11.179	10.898	10.895	1332	4

Notes: Relation between transverse displacements $\overline{w} = \frac{100Ew}{\left(\frac{b}{h}\right)^4 hp_z}$ in $[a/2, b/2, 0]$ and length-to-thickness ratios with 2D formulation using T5 kinematic model and full integration scheme. N^{o}_{FEM} is the number of finite elements.

TABLE 10 Metallic shell.

R_β/h	4	10	50	100	1000	DOF	N^o_{FEM}
Element type							
Exact —	**2.1132**	**1.7798**	**1.6763**	**1.6669**	**1.6591**	—	—
T5							
L4	2.1008	1.6903	0.7319	0.2707	0.0032	1332	36
J1	2.1008	1.6903	0.7319	0.2707	0.0032	1332	36
L9	2.1212	1.7794	1.6639	1.6345	0.7377	1350	12
J2	2.1213	1.7798	1.6691	1.6476	0.9912	1314	14
L16	2.1214	1.7802	1.6761	1.6661	1.6277	1368	6
J3	2.1214	1.7802	1.6763	1.6668	1.6538	1368	9
J4	2.1214	1.7802	1.6764	1.6669	1.6591	1386	6
J5	2.1214	1.7803	1.6764	1.6669	1.6591	1332	4

Notes: Relation between transverse displacements $\overline{w} = \frac{10Ew}{\left(\frac{R_\beta}{h}\right)^4 hp_z}$ in $[a/2, b/2, 0]$ and radius-to-thickness ratios with shell formulation using T5 kinematic model and full integration scheme. N^o_{FEM} is the number of finite elements.

The following considerations can be drawn:

- Shape functions with the same polynomial order present similar results, for example, second-order elements L9 and J2. Furthermore, L4 and J1 present the same results.
- L4 and J1 are progressively far from the reference solution when the length-to-thickness ratio increases. Locking problems also affect L9 and J2, especially for very thin cases. J2 shows slightly better behavior than L9.
- Shear locking is present also for L16 and J3, especially for $R_\beta/h = 1000$. Again, Jacobi shape function performs better.
- J4 and J5 can approach the reference solution for each length-to-thickness ratio, showing that they are locking-free.

7 | ANALYSIS OF PLATES AND SHELLS USING HIGHER-ORDER BEAM THEORIES

In this section, the advanced capabilities of beam formulation for the analysis of plates and shells have been studied.

7.1 | Metallic plate

A convergence of transverse displacement for a very thin plate $b/h = 1000$ is performed, see Table 5 for the properties. Concerning the 1D formulation, J2 and J4 are used as shape functions and T2 is adopted for the cross-section. When 2D formulation is studied, J2 and J4 are used as shape functions and T1 is adopted for the cross-section. Full integration scheme is used. For the sake of clearness, the different ways to build 1D and 2D models are shown in Figure 19. The convergence trend is shown in Figure 19.

Then, transverse displacements at the center of the plate are evaluated for three ratios, namely $b/h = 4, 10, 1000$. Table 11 shows the results by using a fourth-order Taylor (T4) kinematics. Furthermore, DOFs and Number of FEs (N^o_{FEM}) are given for comparison purposes.

The following considerations can be drawn:

- Concerning the convergence analysis, the models with the same order show similar trends. This aspect is more evident in the J4 elements.
- Regarding the relation between transverse displacement and length-to-thickness ratios, $J2_{1D}$ and $J2_{2D}$ present locking problems for thinner plates. On the other hand, $J4_{1D}$ and $J4_{2D}$ match the reference solution in every case.

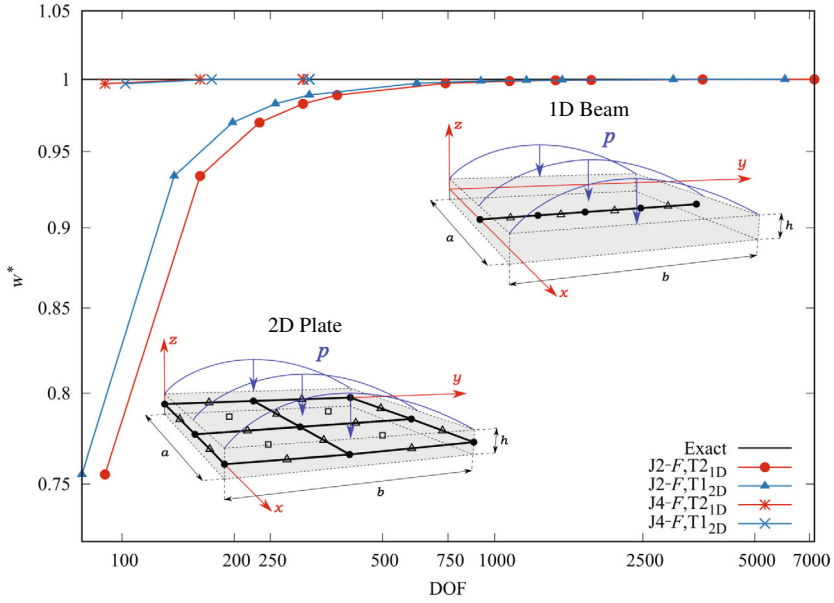

FIGURE 19 Metallic plate, case $b/h = 1000$. Comparison with one- and two-dimensional formulations. Convergence of transverse displacement $w^* = \overline{w}/\overline{w}_{\text{Exact}}$ in $[a/2, b/2, 0]$ by using full integration scheme.

TABLE 11 Metallic plate.

b/h	4	10	1000	DOF	N^o_{FEM}
Element type					
Exact —	**12.656**	**11.179**	**10.895**	—	—
T4					
$J2_{1D}$	12.654	11.166	10.708	765	8
$J4_{1D}$	12.656	11.179	10.895	765	4
$J2_{2D}$	12.655	11.174	10.775	795	10
$J4_{2D}$	12.656	11.179	10.895	795	4

Notes: Comparison for 1D and 2D formulations. Relation between transverse displacement $\overline{w} = \frac{100Ew}{\left(\frac{b}{h}\right)^4 hp_z}$ in $[a/2, b/2, 0]$ and length-to-thickness ratios by using T4 kinematic model and full integration scheme. N^o_{FEM} is the number of finite elements.

- J4 models are not affected by the shear locking, even for a very thin case.

7.2 | Thin-walled cylinder

Finally, a thin-walled cylinder is considered, see Table 5. Concerning the 1D formulation, J2 and J4 are used as shape functions, and T11 is adopted for the cross-section. When 2D shell formulation is studied, J2 and J3 are used as shape functions, and T2 is adopted for the cross-section. Full integration scheme is used. Figure 20 shows the beam and shell FE discretization. Point A is also illustrated. The results are compared with the reference solution.[53] Figure 20 shows the deformed configuration for different models at the midsection. Table 12 shows the transverse displacements evaluated at the Point A. The third and fourth columns report DOFs and Number of FEs (N^o_{FEM}), respectively.

The following considerations can be made:

- Refined models can detect results that are obtainable just by means of shell or solid models in commercial codes and classical formulations, that is, shell-like results can be obtained by means of beam elements.
- Every adopted model is very near to the Nastran shell solution. Some discrepancies from the reference solution are found near loading Point A for both formulations.

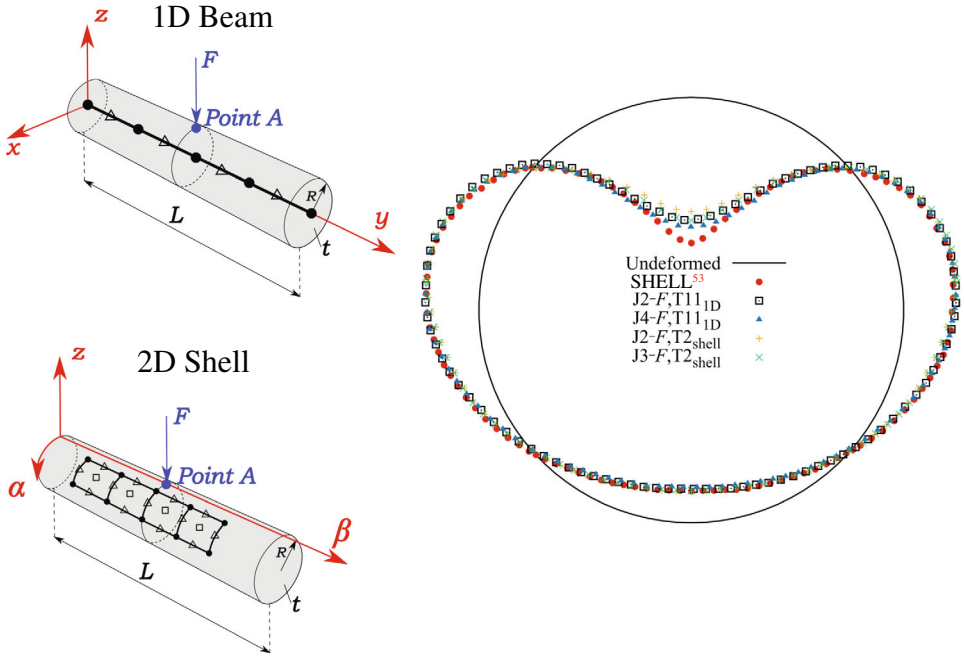

FIGURE 20 Thin-walled cylinder. Comparison for one-dimensional and shell formulations. Deformed cross-section at the midspan of the hollow cylinder.

TABLE 12 Thin-walled cylinder.

Element type	w (m)	DOF	N^o_{FEM}
NASTRAN[53]			
SHELL	−0.670	49,500	—
J2-F,T11$_{1D}$	−0.575	18,954	40
J4-F,T11$_{1D}$	−0.592	18,954	20
J2-F,T2$_{shell}$	−0.537	22,320	40 × 20
J3-F,T2$_{shell}$	−0.578	18,540	20 × 20

Notes: Comparison for one-dimensional and shell formulations. Transverse displacement w in Point A for different finite element method theories. N^o_{FEM} is the number of FEs.

8 | CONCLUSIONS

The present work presented the static analysis of beams, plates and shells by means of Jacobi-like FEs based on the CUF. Various geometries and boundary conditions are considered and 1D beam, 2D plate and shell model are employed.

Four case studies were taken into account. Results are compared with reference analytical and numerical solutions. As far as the convergence rate for the beam case is concerned, it is shown that Jacobi-based on polynomials behave like standard Lagrange-based ones, when they have the same polynomial order. Instead, for the convergence rate of the plates and shells, Lagrange FEs are slightly slower. However, the overall behavior with respect to the shear locking issue is the same and reduced, selective reduced and MITC techniques are adequate to mitigate the problem. For the transverse displacements, the proposed FEs are demonstrated to be reliable with respect to the reference solutions. In particular, the properties of the Lagrange and Jacobi polynomials to build higher order structural theories have been detailed in Carrera et al.[43] Some of the remarks arising from that paper apply to the problem considered in this work, where the same polynomials are used to build several FEs. In fact, given a polynomial order, the results do not depend on the type of the employed polynomial. Finally, the capability of Jacobi-based FEs to build beam models for the analysis of plates and shells is demonstrated.

In this paper, Lagrange and Jacobi polynomials have analogous behavior in the static linear analysis with isotropic materials. The Jacobi polynomials are hierarchical. This means that the domain approximation order can be increased without the need to refine the mesh size. The use of Jacobi shape functions is therefore particularly suggested whenever a consistent convergence analysis is needed, or whenever the analyst needs to conduct a localized detailed analysis. The use of Jacobi shape functions in conjunction with high-order FEs will have further advantages in the study of more complex problems, including the analysis of anisotropic materials or whenever large displacements or strains are considered.

The unified element will be used to test different structural theories and different mesh discretizations/approximations for the problem at hand. Indeed, there are not general rules. The choice of the most consistent structural theory and the most consistent shape function is really problem dependent.

DATA AVAILABILITY STATEMENT

The data that support the findings of this study are available from the corresponding author upon reasonable request.

ENDNOTE

*In the literature, see Reference 40, the following bubble expression, or multiplied by a prefactor, is used for Legendre

$$\phi_j^*(\zeta) = \int_{-1}^{\zeta} P_{j-1}^{\gamma,\theta} d\zeta, \quad j = 2, 3, \ldots, p,$$

but this procedure does not guarantee the condition in Equation (5) for every choices of γ, θ and p.

ORCID

Alfonso Pagani https://orcid.org/0000-0001-9074-2558
Erasmo Carrera https://orcid.org/0000-0002-6911-7763

REFERENCES

1. MacNeal RH. Perspective on finite elements for shell analysis. *Finite Elem Anal Des*. 1998;30:175-186.
2. Euler L. *Methodus Inveniendi Lineas Curvas Maximi Minimive Proprietate Gaudentes Sive Solutio Problematis Isoperimetrici Latissimo Sensu Accepti*. Vol 1. Springer Science & Business Media; 1952.
3. Timoshenko SP. On the transverse vibrations of bars of uniform cross section. *Phil Mag*. 1922;43:125-131.
4. Reddy JN. On locking-free shear deformable beam finite elements. *Comput Methods Appl Mech Eng*. 1997;149(1):113-132.
5. Carrera E, Pagani A, Petrolo M, Zappino E. Recent developments on refined theories for beams with applications. *Mech Eng Rev*. 2015;2(2):14–00298.
6. Bathe KJ. *Finite Element Procedure*. Prentice Hall; 1996.
7. Carrera E, Giunta G, Petrolo M. *Beam Structures: Classical and Advanced Theories*. John Wiley & Sons; 2011.
8. Kirchhoff G. Über das Gleichgewicht und die Bewegung einer elastischen Scheibe. *J Die Reine Angew Math*. 1850;40:51-88.
9. Reissner E. The effect of transverse shear deformation on the bending of elastic plates. *J Appl Mech*. 1945;12:69-77.
10. Mindlin RD. Influence of rotary inertia and shear on flexural motions of isotropic, elastic plates. *J Appl Mech Trans ASME*. 1951;18:31-38.
11. Argyris JH. Matrix displacement analysis of plates and shells, prolegomena to a general theory, part i. *Ing Arch*. 1966;35:102-142.
12. Pryor CW, Baeker RM. A finite-element analysis including transverse shear effects for applications to laminated plates. *AIAA J*. 1971;9(5):912-917.
13. Parisch H. A critical survey of the 9-node degenerated shell element with special emphasis on thin shell application and reduced integration. *Comput Methods Appl Mech Eng*. 1979;20(3):323-350.
14. Bathe KJ, Ho LW. Some results in the analysis of thin shell structures. In: Wunderlich W, Stein E, Bathe KJ, eds. *Nonlinear Finite Element Analysis in Structural Mechanics*. Springer Berlin Heidelberg; 1981:122-150.
15. Carrera E. C0 Reissner–Mindlin multilayered plate elements including zig-zag and interlaminar stress continuity. *Int J Numer Methods Eng*. 1996;39(11):1797-1820.
16. Batoz JL, Bathe KJ, Ho LW. A study of three-node triangular plate bending elements. *Int J Numer Methods Eng*. 1980;15(12):1771-1812.
17. Lee PS, Bathe KJ. The quadratic MITC plate and MITC shell elements in plate bending. *Adv Eng Softw*. 2010;41:712-728.
18. Reddy JN. A penalty plate-bending element for the analysis of laminated anisotropic composite plates. *Int J Numer Methods Eng*. 1980;15(8):1187-1206.
19. Crisfield MA. A quadratic Mindlin element using shear constraints. *Comput Struct*. 1984;18(5):833-852.
20. Zienkiewicz OC, Taylor RL, Too JM. Reduced integration technique in general analysis of plates and shells. *Int J Numer Methods Eng*. 1971;3(2):275-290.
21. Zlàmal M. Superconvergence and reduced integration in the finite element method. *Math Comput*. 1978;143(32):663-685.
22. Prathap G, Bhashyam GR. Reduced integration and the shear-flexible beam element. *Int J Numer Methods Eng*. 1982;18(2):195-210.

23. Hughes TJR, Cohen M, Haroun M. Reduced and selective integration techniques in the finite element analysis of plates. *Nucl Eng Des*. 1978;46(1):203-222.
24. Macneal RH, Harder RL. A proposed standard set of problems to test finite element accuracy. *Finite Elem Anal Des*. 1985;1(1):3-20.
25. Dvorkin E, Bathe KJ. A continuum mechanics based four-node shell element for general nonlinear analysis. *Eng Comput*. 1984;1:77-88.
26. Bucalem ML, Bathe KJ. *The Mechanics of Solids and Structures – Hierarchical Modeling and the Finite Element Solution*. Springer; 2011.
27. Bathe KJ, Dvorkin EN. A formulation of general shell elements—the use of mixed interpolation of tensorial components. *Int J Numer Methods Eng*. 1986;22(3):697-722.
28. Bucalem ML, Bathe KJ. Higher-order MITC general shell elements. *Int J Numer Methods Eng*. 1993;36(21):3729-3754.
29. Cinefra M, Carrera E. Shell finite elements with different through-the-thickness kinematics for the linear analysis of cylindrical multilayered structures. *Int J Numer Methods Eng*. 2013;93(2):160-182.
30. Lee PS, Noh HC, Choi CK. Geometry-dependent mitc method for a 2-node isobeam element. *Struct Eng Mech*. 2008;29(2):2203-2221.
31. Carrera E, Pagani A. Evaluation of the accuracy of classical beam FE models via locking-free hierarchically refined elements. *Int J Mech Sci*. 2015;100:169-179.
32. Carrera E, de Miguel AG, Pagani A. Extension of MITC to higher-order beam models and shear locking analysis for compact, thin-walled, and composite structures. *Int J Numer Methods Eng*. 2017;112(13):1889-1908.
33. Tessler A, Dong SB. On a hierarchy of conforming Tmoshenko beam elements. *Comput Struct*. 1981;14(3):335-344.
34. Tessler A, Hughes TJR. An improved treatment of transverse shear in the Mindlin-type four-node quadrilateral element. *Comput Methods Appl Mech Eng*. 1983;39(3):311-335.
35. Tessler A, Hughes TJR. A three-node Mindlin plate element with improved transverse shear. *Comput Methods Appl Mech Eng*. 1985;50(1):71-101.
36. Tessler A. A C0-anisoparametric three-node shallow shell element. *Comput Methods Appl Mech Eng*. 1990;78(1):89-103.
37. Abramowitz M, Stegun IA. *Handbook of Mathematical Functions with Formulas, Graphs, and Mathematical Tables*. Dover Pubblications; 1964.
38. Beuchler S, Schoeberl J. New shape functions for triangular p-FEM using integrated Jacobi polynomials. *Numer Math*. 2006;103:339-366.
39. Fuentes F, Keith B, Demkowicz L, Nagaraj S. Orientation embedded high order shape functions for the exact sequence elements of all shapes. *Comput Math Appl*. 2015;70(4):353-458.
40. Szabo B, Duester A, Rank E. Chapter 5. The p-version of the finite element method. In: Stein E, de Borst R, Hughes TJR, eds. *Encyclopedia of Computational Mechanics*. John Wiley & Sons, Ltd; 2004; 119-139.
41. Zhu JZ, Zienkiewicz OC. Adaptive techniques in the finite element method. *Commun Appl Numer Method*. 1988;4(2):197-204.
42. Babuška I, Szabo BA, Katz IN. The p-version of the finite element method. *SIAM J Numer Anal*. 1981;18(3):515-545.
43. Carrera E, Augello R, Pagani A, Scano D. Refined multilayered beam, plate and shell elements based on Jacobi polynomials. *Compos Struct*. 2023;304:116275.
44. Carrera E, Giunta G. Refined beam theories based on a unified formulation. *Int J Appl Mech*. 2010;2(1):117-143.
45. Carrera E, Demasi L. Classical and advanced multilayered plate elements based upon PVD and RMVT. Part 1: derivation of finite element matrices. *Int J Numer Methods Eng*. 2002;55(2):191-231.
46. Carrera E, Demasi L. Classical and advanced multilayered plate elements based upon PVD and RMVT. Part 2: numerical implementations. *Int J Numer Methods Eng*. 2002;55(3):253-291.
47. Carrera E. Developments, ideas, and evaluations based upon Reissner's mixed variational theorem in the modeling of multilayered plates and shells. *Appl Mech Rev*. 2001;54(4):301-329.
48. Carrera E, Cinefra M, Li G. Refined finite element solutions for anisotropic laminated plates. *Compos Struct*. 2018;183:63-76. In honor of Prof. Y. Narita.
49. Carrera E. Theories and finite elements for multilayered plates and shells: a unified compact formulation with numerical assessment and benchmarking. *Arch Comput Method Eng*. 2003;10(3):215-296.
50. Carrera E, Cinefra M, Petrolo M, Zappino E. *Finite Element Analysis of Structures through Unified Formulation*. John Wiley & Sons; 2014.
51. Carrera E, Pagani A, Valvano S. Shell elements with through-the-thickness variable kinematics for the analysis of laminated composite and sandwich structures. *Compos Pt B Eng*. 2017;111:294-314.
52. Hughes TJR. *The Finite Element Method: Linear Static and Dynamic Finite Element Analysis*. Courier Corporation; 2012.
53. Carrera E, Giunta G, Petrolo M. Chapter 4. A modern and compact way to formulate classical and advanced beam theories. In: Topping BHV, Adam JM, Pallarés FJ, Bru R, Romero ML, eds. *Developments and Applications in Computational Structures Technology*. Saxe-Coburg Publications; 2010:75-112.
54. Barlow J. Optimal stress locations in finite element models. *Int J Numer Methods Eng*. 1976;10(2):243-251.

How to cite this article: Pagani A, Carrera E, Scano D, Augello R. Finite elements based on Jacobi shape functions for the analysis of beams, plates and shells. *Int J Numer Methods Eng*. 2023;1-30. doi: 10.1002/nme.7316

APPENDIX A. MITC ELEMENTS

This section presents the MITC integration scheme for 1D and 2D formulations. In particular, it is shown that the MITC method is adopted for both Lagrange and Jacobi shape functions. In this work, the same set of tying points is chosen when Lagrange and Jacobi FEs have the same polynomial order. Only beam and shell cases are presented since the plate can be easily derived.

A.1 MITC for beam formulation

For the purposes of the MITC for beam formulation, it is useful to split the strain tensor $\boldsymbol{\epsilon}$ in bending components (with the subscript B) and transverse shear components (with the subscript S) as follows:

$$\boldsymbol{\epsilon}_B = \left\{ \epsilon_{xx} \quad \epsilon_{yy} \quad \epsilon_{zz} \quad \epsilon_{xz} \right\}^T = \left(\mathbf{D}_{B_y} + \mathbf{D}_{B_\Omega} \right) \mathbf{u}, \boldsymbol{\epsilon}_S = \left\{ \epsilon_{yz} \quad \epsilon_{xy} \right\}^T = \left(\mathbf{D}_{S_y} + \mathbf{D}_{S_\Omega} \right) \mathbf{u}. \tag{A1}$$

The definition of differential operators $\mathbf{D}_{B_y}$, $\mathbf{D}_{B_\Omega}$, $\mathbf{D}_{S_y}$, and $\mathbf{D}_{S_\Omega}$ can be found in Reference 32.

If the CUF and FEM approximations for the displacement field $\mathbf{u}$ described in Table 2 are considered, strains can be written as follows:

$$\boldsymbol{\epsilon}_B = F_\tau \left(\mathbf{D}_{B_y} N_i \mathbf{I} \right) \mathbf{q}_{\tau i} + \left(\mathbf{D}_{B_\Omega} F_\tau \mathbf{I} \right) N_i \mathbf{q}_{\tau i}, \quad \boldsymbol{\epsilon}_S = F_\tau \left(\mathbf{D}_{S_y} N_i \mathbf{I} \right) \mathbf{q}_{\tau i} + \left(\mathbf{D}_{S_\Omega} F_\tau \mathbf{I} \right) N_i \mathbf{q}_{\tau i}, \tag{A2}$$

where $\mathbf{I}$ is the identity matrix.

In the MITC method, the bending strains are calculated directly by using the displacements, whereas the transverse shear strains along the beam element are assumed as:

$$\overline{\boldsymbol{\epsilon}}_S = \overline{N}_m \boldsymbol{\epsilon}_{S_m} \qquad m = 1, \ldots, N_n - 1, \tag{A3}$$

where m indicates summation over a set of points, known as tying points, T_m. These points are used to tie the interpolations of the displacements with the assumed strains. The location of these points is given in References 32 and 54. $\boldsymbol{\epsilon}_{S_m}$ is the transverse shear strains vector computed at the tying points by means of Equation (A2). The assumed shear strains vector, $\overline{\boldsymbol{\epsilon}}_S$, is calculated using one tying point for L2 and J1 elements, two for L3 and J2 elements, three for L4 and J3 elements, and so on. In particular, Figures A1A,B shows the tying points for second-order and third-order beam elements, respectively. Finally, the stresses can be expressed by means of the Hooke's Law

$$\overline{\boldsymbol{\sigma}}_B = \mathbf{C}_{BB} \boldsymbol{\epsilon}_B + \mathbf{C}_{BS} \overline{\boldsymbol{\epsilon}}_S, \quad \overline{\boldsymbol{\sigma}}_S = \mathbf{C}_{SB} \boldsymbol{\epsilon}_B + \mathbf{C}_{SS} \overline{\boldsymbol{\epsilon}}_S, \tag{A4}$$

where the material matrices $\mathbf{C}_{BB}$, $\mathbf{C}_{BS}$, $\mathbf{C}_{SB}$, and $\mathbf{C}_{SS}$ can be found in Reference 32.

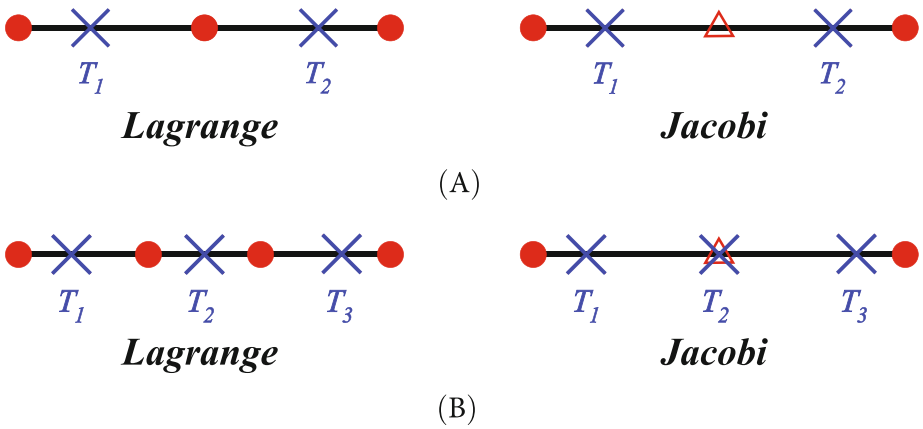

FIGURE A1 Tying points, T_m, for second-order (A) and third (B) beam elements. Definition of nodes ●, edges △ and tying points ×.

A.2 MITC for shell formulation

For the MITC shell elements, the strain are subdivided into in-plane strains, $\boldsymbol{\epsilon}_p$, and out-of-plane strains, $\boldsymbol{\epsilon}_n$. The following relations hold:

$$\boldsymbol{\epsilon}_p = \left\{ \epsilon_{\alpha\alpha} \quad \epsilon_{\beta\beta} \quad \epsilon_{\alpha\beta} \right\}^T = \left(\mathbf{D}_p + \mathbf{A}_p \right) \mathbf{u}, \quad \boldsymbol{\epsilon}_n = \left\{ \epsilon_{\alpha z} \quad \epsilon_{\beta z} \quad \epsilon_{zz} \right\}^T = \left(\mathbf{D}_{n\Omega} + \mathbf{D}_{nz} - \mathbf{A}_n \right) \mathbf{u}. \tag{A5}$$

The definition of differential operators $\mathbf{D}_p$, $\mathbf{A}_p$, $\mathbf{D}_{n_\Omega}$, $\mathbf{D}_{n_z}$, and $\mathbf{A}_n$ can be found in Reference 29.

If the CUF and FEM approximations for the displacement field $\mathbf{u}$ described in Table 2 are considered, strains can be written as follows:

$$\boldsymbol{\epsilon}_p = F_\tau \left(\mathbf{D}_p + \mathbf{A}_p \right) \left(N_i \mathbf{I} \right) \mathbf{q}_{\tau i}, \quad \boldsymbol{\epsilon}_n = F_\tau \left(\mathbf{D}_{n\Omega} - \mathbf{A}_n \right) \left(N_i \mathbf{I} \right) \mathbf{q}_{\tau i} + \left(\mathbf{D}_{n_z} F_\tau \mathbf{I} \right) \mathbf{q}_{\tau i}, \tag{A6}$$

where $\mathbf{I}$ is the identity matrix.

MITC for L4 and J1

For these two elements, the in-plane strains are calculated according to Equation (A6), whereas shear strains are interpolated in the tying points (M, N, P, Q) of the $\xi - \eta$ plane, as indicated in Figure A2, see Reference 27. Assumed out-of-plane strain can be written as follows:

$$\overline{\boldsymbol{\epsilon}}_n = \begin{bmatrix} \frac{1}{2}(1+\xi) & \frac{1}{2}(1-\xi) & 0 & 0 & 0 \\ 0 & 0 & \frac{1}{2}(1+\eta) & \frac{1}{2}(1-\eta) & 0 \\ 0 & 0 & 0 & 0 & 1 \end{bmatrix} \begin{Bmatrix} \epsilon_{\alpha z}^N \\ \epsilon_{\alpha z}^Q \\ \epsilon_{\beta z}^P \\ \epsilon_{\beta z}^M \\ \epsilon_{zz} \end{Bmatrix}. \tag{A7}$$

Finally, the stresses can be expressed by using the Hooke's Law

$$\overline{\boldsymbol{\sigma}}_p = \mathbf{C}_{pp} \boldsymbol{\epsilon}_p + \mathbf{C}_{pn} \overline{\boldsymbol{\epsilon}}_n, \quad \overline{\boldsymbol{\sigma}}_n = \mathbf{C}_{np} \boldsymbol{\epsilon}_p + \mathbf{C}_{nn} \overline{\boldsymbol{\epsilon}}_n, \tag{A8}$$

where the material matrices $\mathbf{C}_{pp}$, $\mathbf{C}_{pn}$, $\mathbf{C}_{np}$, and $\mathbf{C}_{nn}$ can be found in Reference 29.

MITC for L9, L16, J2, and J3

For these four elements, both in-plane and out-of-plane stresses are calculated by using a specific interpolation strategy for each component. The position of tying points is dependent from the element adopted. For the MITC L9 and J2 shell elements, Figure A3 shows the positions of the tying points and their coordinates in the ξ-η plate, see Reference 28.

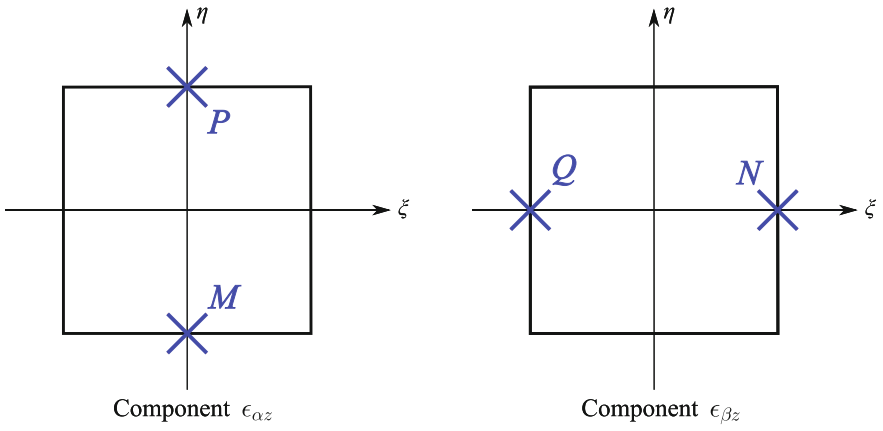

FIGURE A2 Tying points for the mixed interpolation of tensorial components L4 and J1 shell elements.

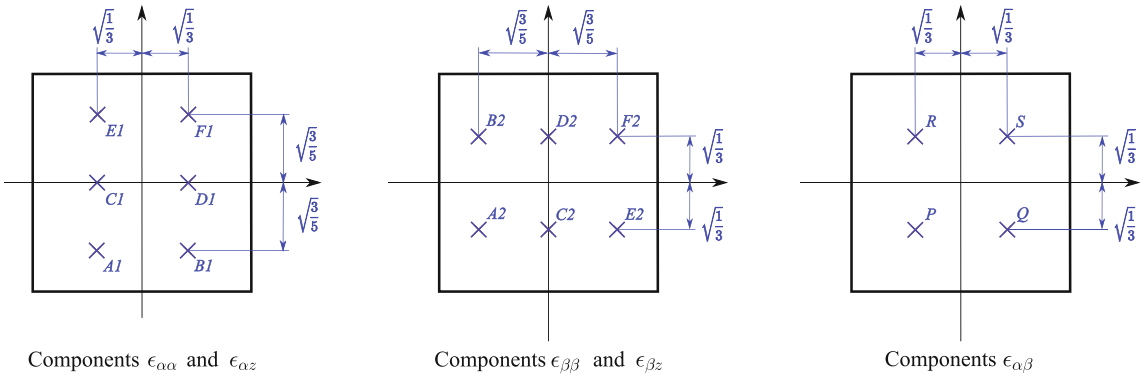

FIGURE A3 Tying points for the mixed interpolation of tensorial components L9 and J2 shell elements.

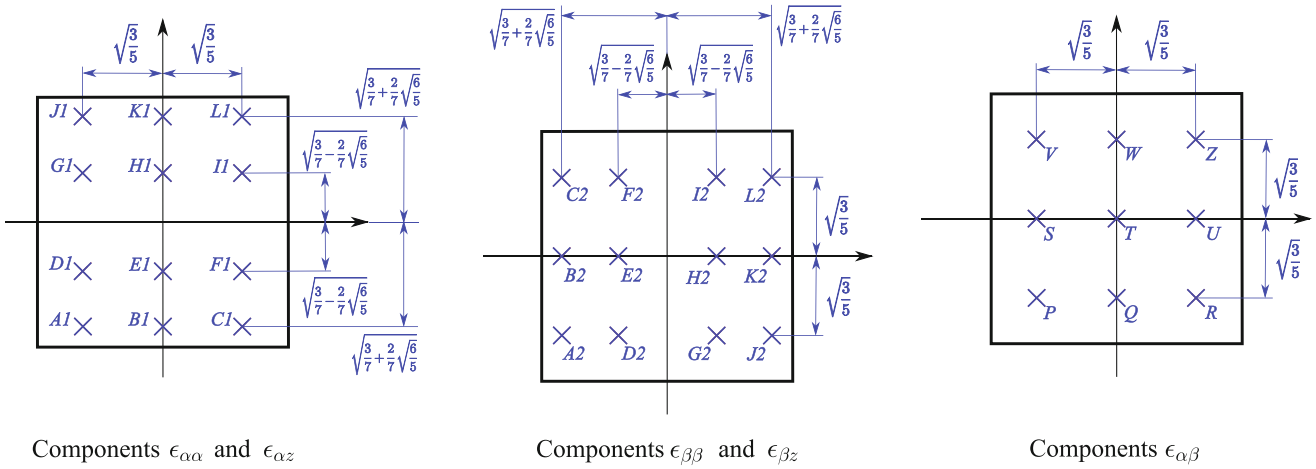

FIGURE A4 Tying points for the mixed interpolation of tensorial components L16 and J3 shell elements.

Lagrangian functions are chosen as the interpolating functions and are arranged in the following arrays:

$$\begin{aligned} N_{m1} &= \begin{bmatrix} N_{A1} & N_{B1} & N_{C1} & N_{D1} & N_{E1} & N_{F1} \end{bmatrix} \\ N_{m2} &= \begin{bmatrix} N_{A2} & N_{B2} & N_{C2} & N_{D2} & N_{E2} & N_{F2} \end{bmatrix} \\ N_{m3} &= \begin{bmatrix} N_P & N_Q & N_R & N_S \end{bmatrix}. \end{aligned} \tag{A9}$$

From this point on, the subscripts $m1$, $m2$, and $m3$ indicate quantities calculated in the points $(A1, B1, C1, D1, E1, F1)$, $(A2, B2, C2, D2, E2, F2)$ and (P, Q, R, S), respectively.

For the MITC L16 and J3 shell elements, Figure A4 shows the tying points and their coordinates in the ξ-η plate, see Reference 28. The Lagrangian interpolating functions are organized as follows:

$$\begin{aligned} N_{m1} &= \begin{bmatrix} N_{A1} & N_{B1} & N_{C1} & N_{D1} & N_{E1} & N_{F1} & N_{G1} & N_{H1} & N_{I1} & N_{J1} & N_{K1} & N_{L1} \end{bmatrix} \\ N_{m2} &= \begin{bmatrix} N_{A2} & N_{B2} & N_{C2} & N_{D2} & N_{E2} & N_{F2} & N_{G2} & N_{H2} & N_{I2} & N_{J2} & N_{K2} & N_{L2} \end{bmatrix} \\ N_{m3} &= \begin{bmatrix} N_P & N_Q & N_R & N_S & N_T & N_U & N_V & N_W & N_X \end{bmatrix}. \end{aligned} \tag{A10}$$

As seen previously for the L9 and J2 elements, the subscripts $m1$, $m2$, and $m3$ indicate quantities calculated in the three sets of points in Figure A4.

Therefore, the strain components are interpolated as follows:

$$\begin{aligned}\overline{\boldsymbol{\epsilon}}_p &= \begin{bmatrix} N_{m1} & 0 & 0 \\ 0 & N_{m2} & 0 \\ 0 & 0 & N_{m3} \end{bmatrix} \begin{Bmatrix} \epsilon_{\alpha\alpha_{m1}} \\ \epsilon_{\beta\beta_{m2}} \\ \epsilon_{\alpha\beta_{m3}} \end{Bmatrix} \\ \overline{\boldsymbol{\epsilon}}_n &= \begin{bmatrix} N_{m1} & 0 & 0 \\ 0 & N_{m2} & 0 \\ 0 & 0 & 1 \end{bmatrix} \begin{Bmatrix} \epsilon_{\alpha z_{m1}} \\ \epsilon_{\beta z_{m2}} \\ \epsilon_{z z_{m3}} \end{Bmatrix},\end{aligned} \tag{A11}$$

where the strains $\epsilon_{\alpha\alpha_{m1}}$, $\epsilon_{\beta\beta_{m2}}$, $\epsilon_{\alpha\beta_{m3}}$, $\epsilon_{\alpha z_{m1}}$, and $\epsilon_{\beta z_{m2}}$ are calculated in the tying points by using (Equation A6).

Finally, the stresses can be expressed by means of the Hooke's Law

$$\overline{\boldsymbol{\sigma}}_p = \mathbf{C}_{pp}\overline{\boldsymbol{\epsilon}}_p + \mathbf{C}_{pn}\overline{\boldsymbol{\epsilon}}_n, \quad \overline{\boldsymbol{\sigma}}_n = \mathbf{C}_{np}\overline{\boldsymbol{\epsilon}}_p + \mathbf{C}_{nn}\overline{\boldsymbol{\epsilon}}_n. \tag{A12}$$